

available at www.sciencedirect.comjournal homepage: www.elsevier.com/locate/chnjc

Review

Progress in research on catalysts for catalytic oxidation of formaldehyde

Bingyang Bai ^{a,b,#}, Qi Qiao ^{a,b}, Junhua Li ^{c,*}, Jiming Hao ^c^a State Key Laboratory of Environmental Criteria and Risk Assessment, Chinese Research Academy of Environmental Sciences, Beijing 100012, China^b Key Laboratory of Eco-Industry of the Ministry of Environmental Protection, Chinese Research Academy of Environmental Sciences, Beijing 100012, China^c State Key Joint Laboratory of Environment Simulation and Pollution Control, School of Environment, Tsinghua University, Beijing 100084, China

ARTICLE INFO

Article history:

Received 27 August 2015

Accepted 20 October 2015

Published 5 January 2016

Keywords:

Formaldehyde

Catalytic oxidation

Metal oxide catalyst

Noble metal catalyst

Low-temperature catalytic activity

ABSTRACT

Formaldehyde (HCHO) is carcinogenic and teratogenic, and is therefore a serious danger to human health. It also adversely affects air quality. Catalytic oxidation is an efficient technique for removing HCHO. The development of highly efficient and stable catalysts that can completely convert HCHO at low temperatures, even room temperature, is important. Supported Pt and Pd catalysts can completely convert HCHO at room temperature, but their industrial applications are limited because they are expensive. The catalytic activities in HCHO oxidation of transition-metal oxide catalysts such as manganese and cobalt oxides with unusual morphologies are better than those of traditional MnO₂, Co₃O₄, or other metal oxides. This is attributed to their specific structures, high specific surface areas, and other factors such as active phase, reducibility, and amount of surface active oxygens. Such catalysts with various morphologies have great potential and can also be used as catalyst supports. The loading of relatively cheap Ag or Au on transition-metal oxides with special morphologies potentially improves the catalytic activity in HCHO removal at room temperature. The preparation and development of new nanocatalysts with various morphologies and structures is important for HCHO removal. In this paper, research progress on precious-metal and transition-metal oxide catalyst systems for HCHO oxidation is reviewed; topics such as oxidation properties, structure–activity relationships, and factors influencing the catalytic activity and reaction mechanism are discussed. Future prospects and directions for the development of such catalysts are also covered.

© 2016, Dalian Institute of Chemical Physics, Chinese Academy of Sciences.
Published by Elsevier B.V. All rights reserved.

1. Introduction

Formaldehyde (HCHO) is a colorless gas with a strong irritating smell at atmospheric pressure. Outdoor HCHO mainly comes from the production of materials such as paints, textiles, printing materials, pesticides, and adhesives, and from motor vehicle exhausts. Indoor HCHO mainly comes from decorating

materials, plywood, fiberboard, particleboard, and other artificial boards [1]. HCHO has serious adverse effects on human health and causes conditions such as edema, eye irritation, headaches, allergic dermatitis, and dark spots. Inhalation of HCHO at high concentrations can induce bronchial asthma, and HCHO can combine with protein amino groups to cause cell mutation. The damage caused by HCHO to human health is

* Corresponding author. Tel/Fax: +86-10-62771093; E-mail: lijunhua@tsinghua.edu.cn# Corresponding author. Tel: +86-10-84914902; Fax: +86-10-84914626; E-mail: baibingyang@tsinghua.org.cn

This work was supported by the National Natural Science Foundation of China (21325731, 51478241, 21221004).

DOI: 10.1016/S1872-2067(15)61007-5 | <http://www.sciencedirect.com/science/journal/18722067> | Chin. J. Catal., Vol. 37, No. 1, January 2016

closely related to its concentration in air and contact time. It has been classified as carcinogenic and teratogenic by the World Health Organization [2,3]. HCHO is also a volatile organic compound (VOC) and has strong photochemical activity, e.g., it can react photochemically with nitrogen oxides (NO_x) [4–7]. HCHO removal is therefore necessary to protect human health and the atmospheric environment.

The main techniques used in the elimination of VOCs are adsorption, and photocatalytic and catalytic oxidation methods [8–21]. Adsorption usually uses activated carbon or molecular sieves as adsorbents for HCHO removal [22–33]. The use of this method is restricted because of the limitations of adsorption capacity and adsorbent regeneration. Photocatalytic methods often use TiO₂-based catalysts to remove HCHO [34–41]. In actual applications, wall paints containing modified TiO₂ catalysts are used. However, under light, such paints can produce secondary pollution of toxicity similar to that of HCHO. Catalytic oxidation is a promising technique, and has advantages such as high removal efficiency, low light-off temperature, wide application scope, simple equipment, and no secondary pollution. HCHO can be directly converted to CO₂ and H₂O [42].

The development of catalytic oxidation techniques is important. The catalytic materials for HCHO oxidation are mainly divided into noble-metal and transition-metal oxide catalyst systems. In this paper, we review progress in research on these two systems in detail, and future directions and potential

hotspots in research on catalysts for HCHO oxidation are discussed.

2. Noble-metal catalysts

Noble-metal catalyst attract much attention because of their excellent low-temperature oxidation activities. They are loaded on supports because precious metals themselves are easily volatilized, oxidized, and sintered. The loading of precious metals on supports enables HCHO conversion at low temperatures. The specific catalytic properties are related to factors such as precious-metal and support types, and structure. The precious-metal catalysts currently used for HCHO oxidation mainly contain Pt, Pd, Au, and Ag as the active components [43]. Other precious metals are not suitable for catalytic combustion because of their high volatilities and ease of oxidation at high temperatures. The supports for precious-metal catalysts for HCHO oxidation can be divided into three types. The first type is materials with no oxidation activities and large specific surface areas, such as SiO₂, Al₂O₃, TiO₂, and molecular sieves; these are common catalyst supports and are commercially available. The second type is single or mixed metal oxides without special morphologies, with high-temperature oxidation activities, but low specific surface areas; examples are bulk CeO₂ and MnO₂; these are traditional metal oxide supports. The third type is metal oxides with special morphologies such as nanorods and

Table 1
Overview of catalytic activities in HCHO oxidation of supported noble-metal catalysts.

Catalysts	Reaction conditions	T ₅₀ (°C)	Ref.
Common supports			
Pt/TiO ₂	100 ppm HCHO, 20 vol% O ₂ , 50000 h ⁻¹ SV	R.T.	[44,45]
Rh/TiO ₂		50	
Pd/TiO ₂		70	
Au/TiO ₂		90	
Na-Pt/TiO ₂	600 ppm HCHO, 20 vol% O ₂ , 300000 h ⁻¹ SV, 50% relative humidity	R.T.	[46]
Na-Pt/TiO ₂	105 ppm HCHO and 315 ppm toluene	R.T.	[47]
Pt/TiO ₂ (C)	36 ppm HCHO, 21 vol% O ₂ , total flow 500 mL/min	R.T.	[48]
Pt/f-SiO ₂	300 ppm HCHO, 20 vol% O ₂ , 30000 mL/(g·h) SV	R.T.	[49]
Pt/SBA-15		40	
Pt/p-SiO ₂		90	
Pt/TiO ₂	100 ppm HCHO, 22 vol% O ₂ , 300000 mL/(g·h) SV	R.T.	[50]
Pd/TiO ₂		80	
Rh/TiO ₂		90	
Pt/SiO ₂		60	
Pt/carbon	100–300 ppm HCHO, 22 vol% O ₂ , 1120 h ⁻¹ SV	<100	[51]
Pt/TiO ₂	10 ppm HCHO, 80000 h ⁻¹ SV, 50% relative humidity	R.T.	[52]
Pd/TiO ₂	10 ppm HCHO, 120000 h ⁻¹ SV, 50% relative humidity	R.T.	[53]
Pd/Bata	40 ppm HCHO, 20 vol% O ₂ , 50000 h ⁻¹ SV, 3% H ₂ O	<40	[54]
Pd/USY		<40	
Pd/ZSM-5		70	
Pd/HM10		>140	
Pd/Zeo-13X		<40	
Pd/Al ₂ O ₃		<40	
PdMn/Al ₂ O ₃	0.5% HCHO, 0.2% CH ₃ OH, 0.7% H ₂ O, 75.6% N ₂ , 23% O ₂	60	[55]
Ag/SBA-15	1000 ppm HCHO, 15 vol% O ₂ , 15000 mL/(g·h) SV	50	[56]
Ag/Al ₂ O ₃	1.2% HCHO, 14.8% O ₂ , 1000 or 7000 h ⁻¹ SV	—	[57]
Ag/SiO ₂			
Ru/Al ₂ O ₃	900 ppm HCHO, 160 ppm CH ₃ OH, 18% H ₂ O, 82% air, 20000 h ⁻¹ SV	198	[58]
Ru/zeolite		210	
Ru/TiO ₂		212	

(To be continued)

Table 1 (Continued)

Catalysts	Reaction conditions	T_{50} (°C)	Ref.
Traditional metal oxide supports			
Pt/CeO ₂	900 ppm HCHO, 160 ppm CH ₃ OH, 18% H ₂ O, 82% air, 20000 h ⁻¹ SV	<150	[58]
Pd/CeO ₂		<150	
Rh/CeO ₂		<150	
Ru/CeO ₂		<150	
Rh/ZrO ₂		188	
Ir/CeO ₂		207	
Ag/CeO ₂	0.42% HCHO, 0.074% CH ₃ OH, 19.9% H ₂ O, 62.7% N ₂ , 16.9% O ₂ , 21000 h ⁻¹ SV	<150	[61]
Pt/MnO _x -CeO ₂	580 ppm HCHO, 20 vol% O ₂ , 30000 mL/(g·h) SV	R.T.	[62]
Ag/MnO _x -CeO ₂	580 ppm HCHO, 18 vol% O ₂ , 30000 mL/(g·h) SV	70	[63]
Ag/CeO ₂		90	
Ag/MnO _x		115	
Pt/CeZrO ₂	100 ppm HCHO, 22 vol% O ₂ , 300000 mL/(g·h) SV	>120	[50]
Pd/Mn-CeO ₂	40 ppm HCHO, 50000 mL/(g·h) SV, 3% H ₂ O	110	[54]
Au/CeO ₂	0.06% HCHO, 32000 mL/(g·h) SV	90	[64]
Au/CeO ₂	500 ppm HCHO, 20 vol% O ₂ , 35400 h ⁻¹ SV	<40	[65]
Au/Fe-O	6.25 mg/m ³ HCHO, 54000 mL/(g·h) SV	40	[66]
Pt/Fe ₂ O ₃	100–500 ppm HCHO, 60000 mL/(g·h) SV	R.T.	[67]
Pt/K-OMS	460 ppm HCHO, 21 vol% O ₂ , 30000 mL/(g·h) SV	>200	[68]
Ag/K-OMS		>200	
Metal oxide supports with special morphologies			
Pt/nest-like MnO ₂	460 ppm HCHO, 20000 mL/(g·h) SV	R.T.	[69]
Ag-HMO	400 ppm HCHO, 10 vol% O ₂ , 30000 mL/(g·h) SV	80	[70,71]
3DOM Au/CeO ₂	0.06% HCHO, 66000 mL/(g·h) SV	70	[72,73]
3DOM Au/CeO ₂ -Co ₃ O ₄	0.06% HCHO (8ppm), 15000 mL/(g·h) SV	R.T.	[74]
3DOM Au/CeO ₂		42	
3DOM Au/Co ₃ O ₄		30	
2D Au/Co ₃ O ₄ -CeO ₂	200 ppm HCHO, 22 vol% O ₂ , 55000 h ⁻¹ SV	R.T.	[75]
2D Au/Co ₃ O ₄		R.T.	
2D Au/CeO ₂		—	
Mesoporous Au/ZrO ₂	90 mg/m ³ HCHO, 52000 mL/(g·h) SV	120	[77]
3D Ag/Co ₃ O ₄	100 ppm HCHO, 20 vol% O ₂ , 30000 h ⁻¹ SV	<80	[78]
3D K-Ag/Co ₃ O ₄		R.T.	
Ag/CeO ₂ nanospheres	810 ppm HCHO, 20 vol% O ₂ , 84000 h ⁻¹ SV	90	[79]
Ag/CeO ₂ bulk particles		140	
Pt-Ce/OMS-2	500 ppm HCHO, 10 vol% O ₂ , 30000 mL/(g·h) SV	120	[80]
Pt/OMS-2		100	

nanospheres, and nanoporous materials; these have better catalytic activities than the corresponding traditional bulk metal oxides. These materials, e.g., MnO₂ nanorods or nanospheres, CeO₂ nanospheres, mesoporous Co₃O₄, and macroporous CeO₂, are metal oxide supports with special morphologies. Table 1 gives an overview of the catalytic activities in HCHO oxidation of various supported noble-metal catalysts.

2.1. Common supports

Common supports used in HCHO oxidation are materials such as SiO₂, Al₂O₃, TiO₂, and molecular sieves. Noble-metal catalysts are often prepared by loading Pt, Pd, Rh, Ru, Au, and Ag on common carriers with large surface areas.

Zhang et al. [44,45] reported TiO₂-supported noble-metal (Pt, Rh, Pd, and Au) catalysts. The order of the HCHO oxidation activities over TiO₂-supported noble-metal catalyst was Pt/TiO₂ > Rh/TiO₂ > Pd/TiO₂ > Au/TiO₂. Complete HCHO conversion to CO₂ and H₂O was achieved over 1% Pt/TiO₂ at 20 °C at a gas hourly space velocity (GHSV) of 50000 h⁻¹ (Fig. 1). High Pt dispersion is an important reason for the high activities. Based on the results achieved using a 1% Pt/TiO₂ catalyst, this research group also prepared 2% Na-1% Pt/TiO₂ using Na⁺

ions as auxiliaries [46]. This catalyst has the best catalytic activity and stability reported to date for HCHO oxidation, and complete conversion is achieved at room temperature for 600 ppm HCHO and a GHSV of 300000 h⁻¹ (Fig. 2). The activity is high because Na⁺ ions generate surface hydroxyl groups for oxidation, and the presence of surface hydroxyl groups changes the reaction mechanism. Nie et al. [47] reported Pt/TiO₂ cata-

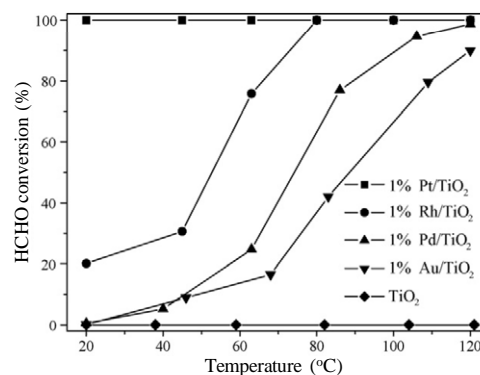


Fig. 1. HCHO conversions on TiO₂-supported 1 wt% noble-metal (Pt, Rh, Pd, and Au) catalysts at various temperatures [45]. Reaction conditions: HCHO 100 ppm, O₂ 20 vol%, He balance, total flow rate 50 mL/min, GHSV 50000 h⁻¹.

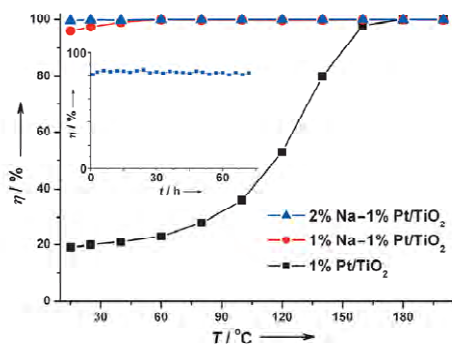


Fig. 2. HCHO conversions over Na-Pt/TiO₂ catalysts [46]. Reaction conditions: HCHO 600 ppm, O₂ 20 vol%, relative humidity 50%, He balance, total flow rate 50 mL/min, and GHSV 120000 h⁻¹ (inset: 2% Na-1% Pt/TiO₂ stability test at 25 °C, GHSV 300000 h⁻¹, other reaction conditions the same).

lysts with various Pt loadings (0.05–2 wt%). They tested their catalytic performances in HCHO oxidation in the presence of toluene. HCHO was selectively oxidized to CO₂ and H₂O by the Pt/TiO₂ catalysts, and toluene did not affect the catalytic reaction. Pt/TiO₂ catalysts prepared with the assistance of NaOH showed higher HCHO oxidation activities than those without NaOH because of the presence of surface hydroxyl groups, high adsorption capacity, and large mesopores and macropores, which facilitate diffusion and transport of reactants and products. Kim et al. [48] reported HCHO oxidation at room temperature on Pt/TiO₂ catalysts. The results show that the catalytic activity depends on the type of TiO₂ carrier, metal valence state of the catalyst, and HCHO feed rate. CO is the main intermediate species in HCHO oxidation. An et al. [49] prepared Pt/SiO₂ and Pt/SBA-15 catalysts; these completely converted HCHO at room temperature and 50 °C, respectively. The use of SiO₂ as a carrier may affect the particle size and chemical valence of Pt species, and this can be favorable to redox reactions of Pt/SiO₂. Peng et al. [50] also prepared supported noble-metal (Pt, Pd, Rh) catalysts. The activity order over TiO₂-based catalysts was Pt/TiO₂ > Pd/TiO₂ > Rh/TiO₂. The activity order for various supports loaded with Pt was TiO₂ > SiO₂ > CeZrO₂. Chuang et al. [51] proposed a reaction mechanism for HCHO oxidation over a Pt catalyst supported on hydrophobic fluorinated carbon. HCHO conversion (T_{50}) over the Pt/carbon catalyst was achieved below 100 °C. Huang et al. [52] prepared Pt/TiO₂ catalysts and examined the effects of metal oxidation state, carrier, and Pt particle size on the catalytic performance in HCHO oxidation. A catalyst consisting of 0.1 wt% Pt/TiO₂ had excellent activity in HCHO oxidation, because the reduction of Pt particles increased electron mobility and the number of reactive oxygen species. This group also prepared Pd/TiO₂ catalysts [53]. These catalysts gave better catalytic performances in HCHO oxidation, with turnover frequencies (TOFs) of 0.015 s⁻¹ at room temperature. Strong metal-support interactions, well-dispersed and negatively charged metallic Pd nanoparticles, and large amounts of chemically adsorbed oxygen are probably responsible for the high catalytic activities. In the reaction, Pd nanoparticles provide active sites for HCHO oxida-

tion, and promote oxygen activation. Park et al. [54] prepared a series of Pd catalysts supported on Bata, USY, ZSM-5, HM10, and Zeo-13X molecular sieves. Pd/ZSM-5, Pd/Bata, Pd/USY, Pd/HM, and Pd/Zeo-13X all have good HCHO catalytic activities at low temperatures ($T_{50} < 40$ °C). The catalytic performance in HCHO oxidation of the Pd/Bata catalyst was slightly better than those of the others. Formate and dioxymethylene are the main intermediates in the reaction, and these are the surface species involved in HCHO oxidation. dela O'Shea et al. [55] prepared a Pd-Mn/Al₂O₃ catalyst, and investigated the effect of feed concentration on its catalytic performance in HCHO/methanol oxidation. Its catalytic activity was low because of decomposition of PdO to Pd and MnO₂/Mn₂O₃ to Mn₃O₄. There were fewer oxygen species available for transfer to Pd⁰. In addition, after water vapor addition, catalyst passivation resulted in competition between water and VOC molecules for active sites. Qu et al. [56] investigated the oxidation of HCHO on a Ag/SBA-15 catalyst. The catalyst completely converted HCHO at 100 °C at a GHSV of 15000 mL/(g·h) (Table 1). This is attributed to higher Ag dispersion in the narrow pores of SBA-15 and high HCHO adsorption. Ag nanoparticles provide active sites for oxidation. In the absence of Ag, HCHO is only converted to formate and dioxymethylene. Mao et al. [57] prepared Ag/Al₂O₃ and Ag/SiO₂ catalysts, and clarified the mechanism of HCHO oxidation. The formation of CO₂ and CO is attributed to the decomposition of formate on the catalyst surface, and the formation of formate is attributed to the reaction of dioxymethylene.

Noble metals loaded on common supports with large surface areas have an excellent catalytic activity. This is related to the specific surface areas of the supports, noble-metal dispersion, active sites, particle size, valence state, and adsorption ability. A large surface area increases exposure of a large number of active sites and the adsorption and diffusion of reactants and products, and can enhance the synergistic effect between the support and the active component. Table 1 shows that the catalytic activities in HCHO oxidation of various noble metals loaded on common supports decrease in the following order: Pt > Pd > Rh > Au > Ag. Pt/TiO₂ [45], and Pd/TiO₂ [53] can completely convert HCHO at room temperature. Na-Pt/TiO₂ is the best catalyst for HCHO removal [46]. Generally, use of a different support but the same active components affects the catalytic activity. For example, Imamura et al. [58] reported the oxidation of HCHO over supported noble-metal catalysts. HCHO conversions (T_{50}) using Ru/Al₂O₃, Ru/zeolite, and Ru/TiO₂ were achieved at 198, 210, and 212 °C, respectively, and conversion with Ru/CeO₂ was obtained below 150 °C. The HCHO oxidation activity of Ru/CeO₂ is better than those of Ru/Al₂O₃, Ru/zeolite, and Ru/TiO₂. For CeO₂ loaded with Ru, Pd, Rh, Pt, and Ir, the order of the catalytic activities (T_{90}) is Ru/CeO₂ > Pd/CeO₂ > Rh/CeO₂ > Ir/CeO₂ > Pt/CeO₂. The better HCHO oxidation activity of the Ru/CeO₂ catalyst indicates that other noble metals, as well as Pt and Pd, may have potential catalytic applications if an appropriate common support is used.

2.2. Traditional metal oxide supports

Catalysts that have the advantages of both precious-metal

and metal oxide catalysts can be obtained by loading precious metals on metal oxide supports. Such catalysts have better low-temperature oxidation activities and thermostabilities, and enhanced interactions between the metal and the support. Sekizawl et al. [59] reported a Pd/SnO₂ catalyst. The results show that the catalyst has a lower specific surface area, but better hydrothermal stability than a Pd/Al₂O₃ catalyst. Minico et al. [60] reported that Au nanoparticles can produce synergies with CeO₂ and Fe₂O₃, reduce the combining capacities of oxygen, Ce, and Fe, strengthen the interactions between Au and the support, and promote reactions with surface oxygen species.

Traditional metal oxide supports for the catalytic oxidation of HCHO, such as CeO₂, Fe₂O₃, Co₃O₄, and MnO₂, or their composites, are usually prepared by precipitation, coprecipitation, or sol-gel methods. Imamura et al. [58,61] reported that supported noble-metal (Ag, Ru, Pd, Rh, and Pt) catalysts all displayed activity in HCHO oxidation below 150 °C. Tang et al. [62] prepared Pt/MnO_x-CeO₂ catalysts and examined the effects of the two precursors on the HCHO oxidation performance. The results show that the activity and stability of the Pt-containing catalyst prepared from Pt(NH₃)₂(NO₂)₂ are better than those of the catalyst prepared from H₂PtCl₆. It can completely oxidize HCHO at room temperature because of effective activation of oxygen molecules on the MnO_x-CeO₂ carrier. A Ag/MnO_x-CeO₂ catalyst was also prepared [63]. Its HCHO oxidation activity (Table 1) is better than those of Ag/MnO_x and Ag/CeO₂. This is attributed to formation of a MnO_x-CeO₂ solid solution and Ag₂O oxygen species produced from a Mn⁴⁺/Mn³⁺ and Ce⁴⁺/Ce³⁺ redox cycle. Shen et al. [64] reported a series of Au/CeO₂ catalysts in which Au clusters are dispersed on the catalyst surfaces. When the Au content is 0.78%, the Au particle size is about 10 nm. The results show that large Au particles are not beneficial to catalytic oxidation. Highly dispersed Au crystallite clusters can provide more active sites for HCHO oxidation. Li et al. [65] also reported the catalytic oxidation of HCHO on Au/CeO₂. An increase in the specific surface area enhanced the catalytic ability. The catalyst has better oxidation activity for two reasons. One is the high valence of Au species on the CeO₂ surface, the other is formation of oxygen vacancies and a Au_xCe_{1-x}O_{2-δ} solid solution. Li et al. [66] prepared a catalyst with Au as the active component and iron oxide as the carrier. The HCHO oxidation activity of the 7.10% Au/Fe-O catalyst ($T_{50} = 40$ °C, Table 1) was the best. This is attributed to the presence of Au^{δ+} and active species that play an important role in the reaction. An et al. [67] reported that Pt/Fe₂O₃ catalysts after calcination at 200 and 300 °C have good activities and stabilities. HCHO can be completely converted at room temperature. This is attributed to interactions between Pt and Fe₂O₃ to form Pt-O-Fe bonds, which are favorable for oxidation. Tian et al. [68] prepared K-OMS-2 using a sol-gel method and loaded Pt and Ag on it using a conventional impregnation method. Unlike the cases for other reported catalysts such as Pt/MnO₂ [69] and Ag/MnO₂ [70], the addition of Pt or Ag reduced the catalytic activity. The order of the catalytic activities in HCHO oxidation was K-OMS-2 > Pt/K-OMS > Ag/K-OMS. HCHO conversion of 50% was achieved over K-OMS-2 at 180 °C.

Among the catalysts of this type listed in Table 1, supported Pt catalysts have excellent catalytic activities (T_{50}) at room temperature. However, some catalysts such as Au/CeO₂, Ag/MnO_x-CeO₂, and Ag/CeO₂ have better development potential, with HCHO conversions (T_{50}) achieved below 40 °C on Au/CeO₂ [65], at 70 °C on Ag/MnO_x-CeO₂, and at 90 °C on Ag/CeO₂ [63]. These results are attributed to stronger interactions between the noble metal and the support, and special crystalline structures with solid solutions. The choice of support is very important for the catalytic activity in HCHO oxidation. The same Au/CeO₂ catalysts [64,65], but with different specific surface areas, show different catalytic activities. Au/CeO₂ with a higher surface area clearly has better oxidation activity ($T_{50} < 40$ °C); the surface area is related to the preparation method. A range of supports are available for supported noble-metal catalysts. Many studies have confirmed that supported Pt catalysts are promising, but limited by the cost of Pt, therefore Pt may not be the best choice as the active component for HCHO removal. Some supported Au and Ag catalysts could be used as alternatives to Pt catalysts. The metal oxide supports can also be modified by using different preparation methods.

2.3. Metal oxide supports with special morphologies

Catalysts supported on metal oxides with special morphologies, which are mainly prepared using hydrothermal and hard template methods, have higher catalytic activities than those supported on conventional bulk metal oxides prepared using precipitation methods. Catalysts with specific morphologies, based on noble metals supported on metal oxides with special morphologies, are better able to remove HCHO at low temperatures, even room temperature, than catalysts with traditional metal oxide supports. Many metal oxides with special morphologies such as tubes, lines, rods, sheets, flowers, spheres, cubes, and pores have been reported, but only metal oxide supports with morphologies involving rods, spheres, mesopores, and macropores have been used in catalytic oxidation of HCHO.

Yu et al. [69] reported a Pt/MnO₂ catalyst with good HCHO oxidation activity. Pt nanoparticles were evenly dispersed on the surfaces of MnO₂ nanospheres. The addition of Pt clearly reduced the reaction temperature. The Pt dispersion, grain size, and interactions between Pt and MnO₂ are the main reasons for the good catalytic activity in HCHO oxidation. Tang's group [70] reported a Ag-hollandite manganese oxide (HMO) catalyst with single Ag atoms as active sites. The HMO nanorods consist of one-dimensional 0.47 × 0.47 nm² square tunnels, and the basic unit of the tunnel structure is built from eight (4 + 4) oxygen atoms to form a tetragonal prism. Each of the eight oxygen atoms in the tunnels has four sp³-hybridized orbitals, three of which bond to three Mn⁴⁺ cations and the other, occupied by lone-pair electrons, points to the central axis of the tunnel. Theoretically, linear tunnels of a specific size and electron-rich tunnel oxygen atoms can serve as a natural mold and an electron donor, respectively; this favors formation of stable single-atom Ag chains in the HMO tunnels. The single Ag atoms

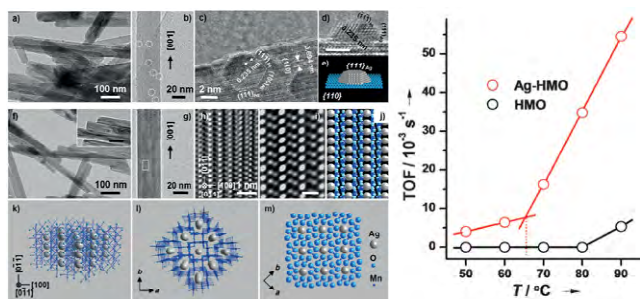


Fig. 3. TEM and high-resolution TEM images and corresponding structural models of Ag-HMO; TOFs for HCHO oxidation over Ag-HMO are taken from Ref. [70].

anchored at the openings of the Ag-HMO tunnel nanorods are active sites, and can easily activate lattice oxygen and molecular oxygen. The Ag-HMO structure is shown in Fig. 3. The activation of oxygen species results in excellent HCHO oxidation activity at low temperatures. The Ag-HMO catalyst has a high TOF, 0.054 s^{-1} , at $90 \text{ }^\circ\text{C}$ and HCHO conversion (T_{50}) is achieved at $80 \text{ }^\circ\text{C}$ (Table 1). This group also examined the atomic Ag centers [71]. Zhang et al. [72] prepared three-dimensional ordered macroporous (3DOM) Au/CeO₂ with controlled pore sizes. Fig. 4 shows scanning electron microscopy (SEM) and transmission electron microscopy (TEM) images, and HCHO conversions for 3DOM 1 wt% Au/CeO₂ prepared using CeO₂ of pore size 80 nm. The catalyst has interconnected networks of spherical voids. Au nanoparticles are uniformly dispersed on the surface. The catalytic activity of 3DOM 1 wt% Au/CeO₂ in HCHO oxidation is excellent and complete conversion of 0.06 vol% HCHO is achieved at $75 \text{ }^\circ\text{C}$. This temperature is lower than that needed for complete conversion using non-porous Au/CeO₂. The better activity of 3DOM Au/CeO₂ in HCHO oxidation is the result of Au dispersion, a higher Au content, and the presence of Au³⁺. This group also reported the mechanism of HCHO oxidation on the 3DOM Au/CeO₂ catalyst [73]. HCHO molecules are adsorbed to form formate species on the catalyst surface. The adsorption and activation of oxygen species are related to the Au³⁺/Au⁰ and Ce⁴⁺/Ce³⁺ redox cycles. During HCHO oxidation, formate species are further oxidized to CO₂ and H₂O by active oxygen species. If the formate is not completely oxidized, carbonate or bicarbonate is produced on the 3DOM Au/CeO₂ surface, and may cause catalyst passivation. However, it is difficult to block the active sites on the catalyst

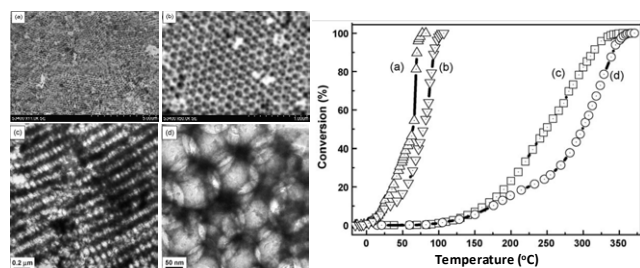


Fig. 4. SEM and TEM images of 3DOM Au ~1 wt%/CeO₂; HCHO conversions of (a) 3DOM Au ~1 wt%/CeO₂ (80 nm pore size), (b) 3DOM Au ~1 wt%/CeO₂ (130 nm pore size), (c) 3DOM CeO₂ (80 nm pore size), (d) 3DOM CeO₂ (130 nm pore size) from Ref. [72].

surface because of the large and open pores. A 3DOM Au/CeO₂-Co₃O₄ catalyst was prepared by this group, based on 3DOM Au/CeO₂ [74]. HCHO can be completely converted at $39 \text{ }^\circ\text{C}$. The interactions between CeO₂ and Co₃O₄ promote the migration of surface oxygen species and activation of Au species. Ma et al. [75] reported that two-dimensional (2D) ordered mesoporous Au/Co₃O₄-CeO₂ had good catalytic activity in HCHO oxidation, with 50% HCHO conversion at room temperature (Table 1). The catalytic activity decreases with increasing CeO₂ content. The (110) crystal planes of Co₃O₄ are the main active faces, and they can adsorb and activate HCHO species. Au loading facilitates the formation of surface oxygen species. This group also prepared a similar 3D Au/Co₃O₄ catalyst for the elimination of ethylene, and a better catalytic performance was obtained [76]. Zhang et al. [77] prepared mesoporous Au/ZrO₂ for HCHO oxidation. The Au is better dispersed, with more Au³⁺ ions and a stronger HCHO adsorption ability. The Au³⁺ ions are reduced to Au⁰ metal, and adsorbed HCHO molecules are quickly converted to formate species. A catalysts consisting of 0.85 wt% Au/ZrO₂ can completely convert HCHO at $180 \text{ }^\circ\text{C}$ because of adsorption of HCHO on Au species and of oxygen molecules on the support.

Our group used KIT-6 mesoporous silica as a hard template to prepare 3D ordered Co₃O₄ [42]. Mesoporous metal oxides have potential as catalysts. Mesoporous Ag/Co₃O₄ and K-Ag/Co₃O₄ catalysts based on 3D Co₃O₄ were prepared [78]. Ag nanoparticles were uniformly dispersed and supported on a polycrystalline wall. The addition of K⁺ ions strengthens anionic lattice defects and interactions between Ag and the Co₃O₄ support, resulting in formation of more Co³⁺ ions and surface lat-

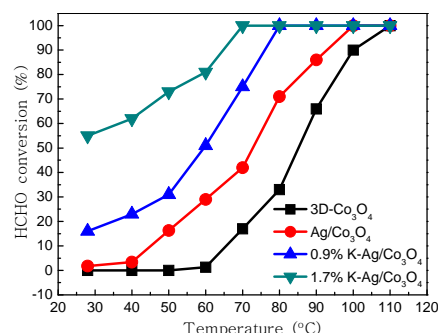


Fig. 5. HCHO conversion over K-Ag/Co₃O₄ catalyst [78].

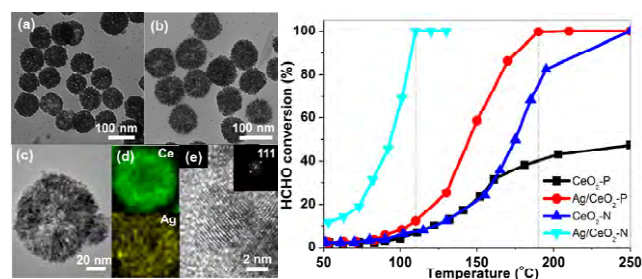


Fig. 6. TEM image of (a) CeO₂-N nanosphere, (b) Ag/CeO₂-N nanosphere, (c) Ag/CeO₂-N nanosphere, (e) Ag/CeO₂-N nanosphere and (d) the distribution of element maps of Ce (green) and Ag (yellow) on Ag/CeO₂-N nanosphere and HCHO conversions over Ag/CeO₂ nanospheres [79].

tice oxygen species. The catalytic activity in HCHO oxidation of the K-Ag/Co₃O₄ sample is better than that of the Ag/Co₃O₄ catalyst because of the presence of surface hydroxyl species and exposure of Ag (111) active faces. HCHO conversion of 50% was achieved at room temperature using K-Ag/Co₃O₄ (Fig. 5). Our group reported catalysts with Ag nanoparticles loaded on CeO₂ nanospheres and bulk particles [79]. Fig. 6 shows TEM images of the Ag/CeO₂ nanospheres and the achieved HCHO conversions. The catalytic activity in HCHO oxidation of Ag/CeO₂ nanospheres is better than that of Ag/CeO₂ bulk particles. Ag/CeO₂ nanospheres can completely convert 810 ppm HCHO at 110 °C and a GHSV of 84000 h⁻¹; the HCHO conversion (*T*₅₀) at 90 °C is shown in Table 1. The reaction rate is almost 3.6 times that obtained with Ag/CeO₂ bulk

particles. The average Ag/CeO₂ nanosphere size is between 80 and 100 nm, and it consists of small crystallites of size 2–5 nm. This special structure promotes good distribution of Ce and Ag. Oxygen is easily chemisorbed on the Ag/CeO₂ nanosphere surfaces, and interactions between Ag and CeO₂ may occur in the catalyst. Our group also reported that the catalytic activity of Pt-Ce/OMS-2 in HCHO oxidation [80] was lower than those over Ag-HMO [70], K-Ag/Co₃O₄ [78], and Ag-CeO₂ nanospheres [79].

Table 1 shows that metal oxide supports with special structures have rarely been used for Pt loading, except Pt/nest-like MnO₂ [69] and Pt/OMS-2 [80]. This is because 2% Na-1% Pt/TiO₂ has become the benchmark for supported Pt catalysts, and is used in air purification. More attention has been paid to

Table 2

Overview of catalytic activities of transition-metal oxides in HCHO oxidation.

Catalysts	Reaction conditions	<i>T</i> ₅₀ (°C)	Ref.
Single metal oxide catalysts			
MnO ₂ , Ag ₂ O, PdO, CoO, CuO, ZnO, Fe ₂ O ₃ , La ₂ O ₃ , V ₂ O ₅ , TiO ₂ , CeO ₂ and Mn ₃ O ₄	<750 ppm HCHO	—	[81,82]
Cryptomelane	100 ppm HCHO, 20 vol% O ₂ , 50000 h ⁻¹ SV	90	[83]
Birnessite		95	
Ramsdellite		100	
MnOOH nanorods		115	
Pyrolusite	400 ppm HCHO, 10 vol% O ₂ , 18000 mL/(g·h) SV	150	[84]
Cryptomelane		110	
Todorokite		140	
Cocoon-like MnO ₂	460 ppm HCHO, 20000 mL/(g·h) SV	130	[69]
Urchin-like MnO ₂		120	
Nest-like MnO ₂		110	
Hollow K _x MnO ₂	100 ppm HCHO, 20 vol% O ₂ , 50000 h ⁻¹ SV	50	[88]
Honeycomb MnO ₂		70	
OMS-2 nanorods	0.01% HCHO, 20 vol% O ₂ , 24000 mL/(g·h) SV	75	[89]
MnO _x		85	
OMS-2	500 ppm HCHO, 10 vol% O ₂ , 30000 mL/(g·h) SV	110	[80]
OMS-2 nanoparticles	460 ppm HCHO, 21 vol% O ₂ , 20000 mL/(g·h) SV	90	[90]
OMS-2 nanorods		>100	
Birnessite MnO ₂	460 ppm HCHO, 21 vol% O ₂ , 30000 mL/(g·h) SV	80	[91]
3D-Cr ₂ O ₃	500 ppm HCHO, 30000 mL/(g·h) SV	92	[92]
3DOM CeO ₂	0.06% HCHO, 66000 mL/(g·h) SV	250	[72]
3D-Co ₃ O ₄	400 ppm HCHO, 20 vol% O ₂ , 30000 mL/(g·h) SV	<110	[42]
2D-Co ₃ O ₄		<130	
Co ₃ O ₄ nanopaticles		<210	
CeO ₂ nanospheres	810 ppm HCHO, 20 vol% O ₂ , 84000 h ⁻¹ SV	175	[79]
CeO ₂ bulk particles		>250	
3D-MnO ₂	400 ppm HCHO, 20 vol% O ₂ , 30000 mL/(g·h) SV	<100	[94]
α-MnO ₂ nanorods		100	
β-MnO ₂ nanorods		>140	
Composite metal oxide catalysts			
MnO _x -CeO ₂ (Mn/Ce = 1)	580 ppm HCHO, 20 vol% O ₂ , 30000 mL/(g·h) SV	<90	[62]
	580 ppm HCHO, 18 vol% O ₂ , 21000 mL/(g·h) SV		[95]
	580 ppm HCHO, 20 vol% O ₂ ,	150	[96]
CeMn10		125	
CeMn30		100	
CeMn50		80	
CeMn80		72	
MnO _x		225	
CeO ₂		150	[97]
MnO _x -SnO ₂	400 ppm HCHO, 10 vol% O ₂ , 30000 mL/(g·h) SV	<120	[98]
CuO/MnO ₂	0.18–1.3 ppm HCHO, 100000 h ⁻¹ SV	170	[99]
Co(N)/Zr	150 ppm HCHO, 20 vol% O ₂ , 30000 mL/(g·h) SV	155	
Co-CD _{0.1} /Zr		—	[100]
Mesoporous Co-Mn	80 ppm HCHO, 36000 h ⁻¹ SV, 50% relative humidity	—	[75]
Mesoporous Co ₃ O ₄ -CeO ₂	200 ppm HCHO, 22 vol% O ₂ , 55000 h ⁻¹ SV	—	

catalysts consisting of Ag and Au loaded on metal oxide supports with special morphologies. Such catalysts, e.g., mesoporous 3DOM Au/CeO₂-Co₃O₄ [74], 2D Au/Co₃O₄-CeO₂, 2D Au/Co₃O₄ [75], and 3D K-Ag/Co₃O₄ [78], all have excellent catalytic activities in HCHO oxidation at room temperature (T_{50} = room temperature) and have good potential applications. The interactions between the noble metal and the support, dispersion, particle size, low-temperature reducibility, mobility and activation of active oxygen species, and redox cycles of high- and low-valence states of metal ions are responsible for the excellent catalytic activities in HCHO oxidation. Experimental results have shown that Au and Ag, which are cheaper than Pt and Pd, can provide sufficient active sites for HCHO oxidation (Table 1). Catalysts with Au and Ag on supports with special morphologies, especially porous structures, are promising for HCHO removal at room temperature and may become substitutes for Pt catalysts.

3. Transition-metal oxide catalytic systems

Precious-metal catalysts have excellent low-temperature catalytic activities in HCHO oxidation, but their industrial use is restricted because of their high costs. Precious-metal catalysts have poor thermal stabilities at 500–900 °C. These catalysts are easily sintered, resulting in decreased surface area, which decreases their catalytic activities. Transition-metal oxides are cheap and plentiful, and transition-metal oxide catalysts have potential applications in VOC removal. Transition-metal oxide catalysts with good thermal stabilities have therefore attracted much attention. Transition-metal oxide catalysts with good activities ($T_{100} \leq 140$ °C) in HCHO oxidation mainly contain Mn, Co, and Cr. Other metal elements such as Ce, Sn, Cu, and Zr can be doped into MnO_x and Co₃O₄ to prepare composite metal oxides if a single metal oxide does not give a good catalytic performance. In addition, a single rare-earth oxide, i.e., CeO₂, has been used in the catalytic oxidation of HCHO. Table 2 gives an overview of the catalytic activities of transition-metal oxides in HCHO oxidation.

3.1. Single metal oxide catalysts

In 2001, Sekine et al. [81] developed a cardboard-like air purification material composed mainly of activated carbon particles and MnO_x. The material was tested by many families in Japan. This material reduced indoor HCHO concentrations from 0.21 to 0.04 ppm, and desorbed HCHO molecules from indoor building materials. In 2002, Sekine [82] also reported catalytic HCHO oxidations using various metal oxides such as Ag₂O, PdO, CoO, CuO, ZnO, Fe₂O₃, La₂O₃, V₂O₅, MnO₂, TiO₂, CeO₂, and Mn₃O₄. Apart from those with La₂O₃, ZnO, and CuO, Fe₂O₃, and V₂O₅, the HCHO conversion rates of these oxides were above 50%. MnO₂ showed the best catalytic activity. The catalytic activities of two types of MnO₂ were tested. The catalytic performance of the MnO₂ sample with a higher specific surface area was better, because a higher specific surface area is conducive to the adsorption and oxidation of gas-phase components. The MnO₂ catalyst contains multi-holes, therefore oxy-

gen molecules can easily spread to the active sites on the surface, giving complete HCHO conversion at 100 °C.

Since 2002, most research has focused on MnO₂ catalysts for HCHO oxidation because its catalytic activity is better than those of other oxides such as CuO, Fe₂O₃, La₂O₃, V₂O₅, TiO₂, and CeO₂. MnO₂ has various morphologies, namely α , β , γ and δ types. Zhou et al. [83] used a hydrothermal method to prepare MnO₂ samples consisting of cryptomelane, birnessite, and ramsdellite, and monoclinic crystalline MnOOH nanorods. Of these, cryptomelane MnO₂ has the best catalytic properties. Chen et al. [84] prepared pyrolusite, cryptomelane, and todorokite manganese oxides with different channel structures. The catalytic activity of cryptomelane MnO₂ is better than those of the others (Fig. 7). The effect of pore channels in HCHO oxidation is stronger than those of crystallinity, specific surface area, reducibility, and Mn oxidation state. Cryptomelane has the best catalytic activity mainly because the HCHO molecules and pore channels are of similar size. It has been reported in Ref. [83,84] that the crystalline structure of a catalyst determines its catalytic activity.

Experimental and theoretical results have shown that the catalytic oxidation activity is affected by factors such as structure, specific surface area, active oxygen species, and active phase [85–87]. Most metal oxides synthesized by traditional precipitation methods have relatively small specific surface areas, fewer exposed active sites or oxygen species, and poor low-temperature reducibility. These limitations are a drawback in catalytic oxidation of HCHO. Properties such as a large specific surface area, good low-temperature reducibility, and large number of active sites enhance the catalytic ability. Materials containing the same components, but with different morphologies and structures, have different functions. Researchers are now trying to change the structures and morphologies of metal oxides to control the factors that influence their catalytic activities.

MnO₂ synthesized with various morphologies such as rods, spheres, particles, and porous have enhanced catalytic properties. Yu et al. [69] prepared MnO₂ materials with cocoon, sea-urchin, and nest morphologies (Fig. 8). Nest-like MnO₂ has the best HCHO oxidation activity because of its hole structure, which is beneficial for the adsorption and transformation of HCHO. The MnO₂ nests have diameters in the range 1–3 μ m, and consist of nanorods of width 10–50 nm and length 0.2–1.5 μ m. Chen et al. [88] reported that hollow K_xMnO₂ nanospheres

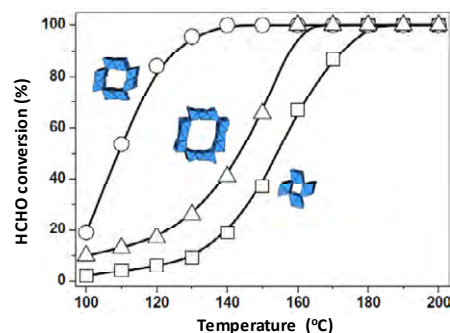


Fig. 7. Complete oxidation of HCHO on pyrolusite, cryptomelane, and todorokite manganese oxides [84].

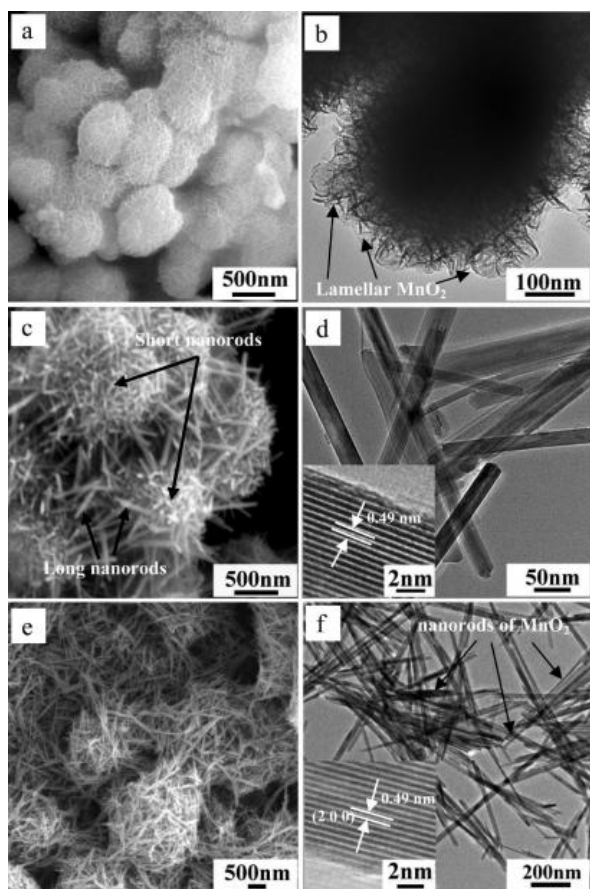


Fig. 8. SEM (a, c, e) and TEM (b, d, f) images of three MnO₂ nanostructures: (a, b) cocoon-like MnO₂, (c, d) sea-urchin-like MnO₂, (e, f) nest-like MnO₂ [69].

gave good catalytic performance in low-temperature HCHO oxidation, with complete conversion at 80 °C. The catalytic activity of this material is superior to those of OMS-2, traditional MnO_x powder, and Mn–Pd/Al₂O₃. The structure and HCHO conversion data for the catalyst are shown in Fig. 9. Tang et al. [89] reported that the catalytic performance of OMS-2 nanorods with a molecular sieve structure consisting of octahedral Mn was better than that of traditional MnO_x. Tian et al. [90] prepared K-OMS-2 nanoparticles with an octahedral Mn structure; its HCHO oxidation activity was superior to that of OMS-2 nanorods. This group [91] also prepared MnO_x catalysts with a birnessite structure; they had excellent catalytic activities in

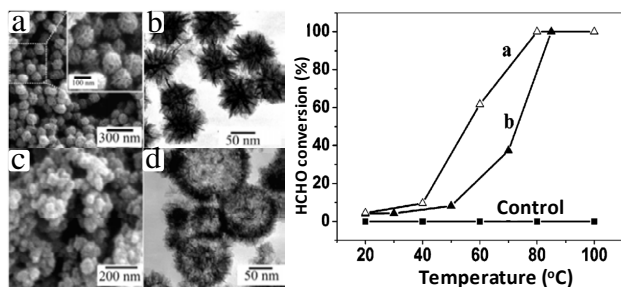


Fig. 9. SEM and TEM images of honeycomb K_xMnO₂ nanospheres (a,b) and hollow K_xMnO₂ nanospheres (c,d); HCHO conversions over hollow K_xMnO₂ nanospheres (a) and honeycomb K_xMnO₂ nanospheres (b) [88].

HCHO oxidation because of the special topography, large surface area, and good surface reducibility.

Morphological changes can improve the factors that influence catalytic activity, such as the specific surface area, low-temperature reducibility, and active phase. Research has not been confined to MnO₂ materials with various structures and morphologies. Other transition-metal oxides (Cr₂O₃ and Co₃O₄) and a rare-earth oxide (CeO₂) have been studied. Xia et al. [92] reported the use of 3D ordered mesoporous Cr₂O₃ in catalytic oxidation of HCHO. The TEM images in Fig. 10 show the mesoporous structure of the catalyst. Mesoporous Cr₂O₃ calcined at 400 °C has the best HCHO oxidation activity, and complete HCHO conversion is achieved at 130 °C with 500 ppm HCHO and a GHSV of 30000 mL/(g·h) (Fig. 10). The activation energy is 45.6 kJ/mol. The specific surface area of mesoporous Cr₂O₃ (69–124 m²/g) is larger than that of traditional bulk Cr₂O₃; it also has better low-temperature reducibility, which enhances its catalytic properties. The catalytic activity is also related to the catalyst preparation process and the template quality. Zhang et al. [72] reported a 3DOM CeO₂ catalyst with a controllable pore size. The catalytic activity in HCHO oxidation of a catalyst with a pore diameter of 80 nm is better than that of one with a pore diameter of 130 nm; it has a larger surface area and can completely convert HCHO to CO₂ and H₂O at 355 °C.

Our group used SBA-15 and KIT-6 as hard templates to prepare 2D Co₃O₄ and 3D Co₃O₄ catalysts [42]. The materials have the structural characteristics of their templates, and contain 2D hexagonal (p6mm) pore channel structures and 3D symmetrical cubic (ia3d) structures, respectively. These materials all have the crystalline cobalt oxide spinel structure. The 3D Co₃O₄ catalyst gave 100% HCHO conversion at 130 °C and a space velocity of 30000 mL/(g·h). The 2D Co₃O₄ catalyst oxidized HCHO completely at 140 °C under the same space velocity conditions (Fig. 11). The difference between the activities of these catalysts arises from the channel structure of the mesoporous Co₃O₄ prepared using the hard template method; it has a high specific surface area and a large number of surface-active species, enabling reactants to diffuse and undergo surface reactions. The Brunauer–Emmett–Teller specific surface areas of 2D Co₃O₄ and 3D Co₃O₄ are 43.3 and 85.9 m²/g, respectively; these values are much larger than that of traditional nano-Co₃O₄ (28.1 m²/g). A catalyst with a larger specific surface area exposes more active facets during oxidation. TEM images show that the active faces of 3D Co₃O₄ are (220) crystal

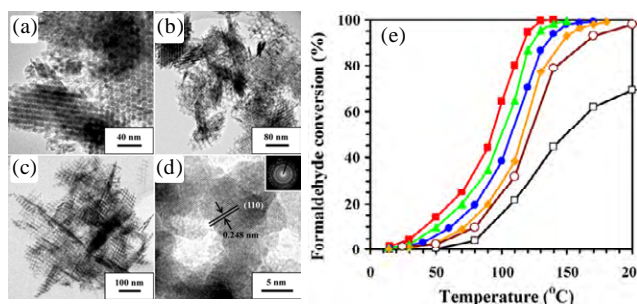


Fig. 10. TEM images (a–d) and HCHO conversions (e) over 3D Cr₂O₃ catalyst [92].

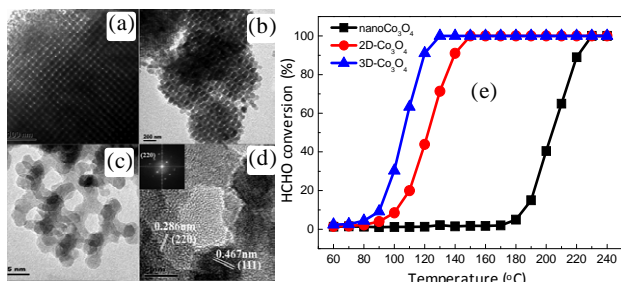


Fig. 11. TEM images (a–d) and HCHO conversions (e) over 3D Co_3O_4 catalyst [42].

planes (Fig. 11), which mainly consist of abundant Co^{3+} ions, which provide sufficient active sites for oxidation. Large numbers of Co^{3+} ions are exposed on its surface, further enhancing the catalytic ability. X-ray photoelectron spectroscopy shows that greater quantities of Co^{3+} ions are present on the surface of 3D Co_3O_4 than on that of 2D Co_3O_4 . A larger number of Co^{3+} species can increase the number of anionic defects, and this promotes adsorption and activation of oxygen in the gas phase. Oxygen temperature-programmed desorption shows that mesoporous Co_3O_4 , particularly 3D Co_3O_4 , has a large number of surface-active oxygen species, which are easily stripped off and quickly filled by gas-phase oxygen. This improves the oxidation capacity. Larger surface areas, more abundant surface-active oxygen species, and a larger amount Co^{3+} active species are responsible for the improved oxidation activity. Our group also prepared CeO_2 nanospheres [79]. The catalytic activity of CeO_2 nanospheres in HCHO oxidation is better than that of traditional bulk CeO_2 nanoparticles (Fig. 6). The HCHO conversion rate with CeO_2 nanospheres is 85% at 200 °C, whereas that of bulk CeO_2 nanoparticles is only 40%. This is because CeO_2 nanospheres have a larger specific surface area (148.6 m^2/g) than bulk CeO_2 (57.8 m^2/g). A morphological change can increase the specific surface area or affect other factors that influence the catalytic activity in HCHO oxidation, and can therefore enhance the oxidation performance. Our group [93,94] reported that the catalytic activity of a 3D ordered mesoporous MnO_2 catalyst ($T_{100} < 140$ °C) in HCHO and ethanol oxidation is better than that of MnO_2 nanorods because it contains more Mn^{4+} ions as the active phase and has a higher specific surface area.

Table 2 shows that single metal oxide catalysts such as MnO_2 nanorods, cryptomelane nanospheres, and mesoporous MnO_2 , Co_3O_4 , and Cr_2O_3 have good catalytic activities in HCHO oxidation, and their T_{50} and T_{100} HCHO conversions are less than or equal to 110 and 140 °C, respectively. Their catalytic activities are superior to those of traditional metal oxide catalysts synthesized using precipitation methods. This is because these catalysts have special morphologies and structures and high surface areas, which promote HCHO activation on the catalyst surface. Morphological changes can increase the surface area and, more importantly, increase the low-temperature reducibility, and numbers of active cations and surface-active oxygen species, and therefore increase the oxidation ability of the catalyst. Single metal oxide catalysts with special morphol-

ogies have a range of potential applications because they are cheap and give good catalytic performances.

3.2. Composite metal oxide catalysts

The development of transition-metal oxide catalysts that can completely convert HCHO at room temperature is desirable. Some single metal oxides cannot convert HCHO at low temperatures; other elements such as Ce, Sn, Zr, and Cu have been added to manganese and cobalt oxides to prepare Mn- and Co-based catalysts.

Tang et al. [62] used a coprecipitation method to prepare a $\text{MnO}_x\text{-CeO}_2$ mixed oxide, and investigated the effect of the $\text{Mn}/(\text{Mn} + \text{Ce})$ molar ratio on its catalytic performance in HCHO oxidation. The best catalytic activity was obtained when the Mn/Ce mole ratio was 1:1. HCHO conversion of 90% was achieved at 90 °C with a 580 ppm feed concentration and space velocity of 30000 $\text{mL}/(\text{g}\cdot\text{h})$. Formation of a solid solution and improved reducibility are responsible for the good catalytic performance. Tang et al. [95] also reported Mn–Ce catalysts. A $\text{MnO}_x\text{-CeO}_2$ sample prepared using a modified coprecipitation method completely converted HCHO at 100 °C at 580 ppm HCHO and a GHSV of 21000 $\text{mL}/(\text{g}\cdot\text{h})$ (Fig. 12). The large number of Mn^{4+} ions and surface lattice oxygen species are responsible for the excellent catalytic activity in HCHO oxidation. Liu et al. [96] also prepared a $\text{MnO}_x\text{-CeO}_2$ catalyst. The average oxidation state of Mn species on the catalyst surface was higher than that of pure MnO_x . An improved catalytic performance in HCHO oxidation was achieved because of activation of surface lattice oxygen species. Wen et al. [97] reported the preparation of $\text{MnO}_x\text{-SnO}_2$ catalysts using a coprecipitation method. These gave good catalytic performances in HCHO oxidation because of the presence of high-oxidation-state Mn species and the formation of a Mn–Sn solid solution. Pei et al. [98] reported the performance and kinetics of a CuO/MnO_2 catalyst for indoor HCHO removal. The experimental data for HCHO oxidation over the CuO/MnO_2 catalyst fitted the traditional Langmuir–Hinshelwood model.

Bai et al. [99] used cyclodextrin (CD) to prepare a $\text{Co}_3\text{O}_4/\text{Zr}$ catalyst. The catalytic performance of the material containing CD and Co in a molar ratio of 0.1:1 was better than that of a catalyst directly prepared from cobalt nitrate; this is attributed

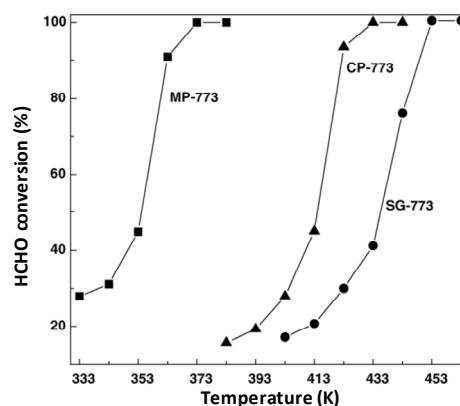


Fig. 12. HCHO conversions over various $\text{MnO}_x\text{-CeO}_2$ catalysts [95].

to stronger interactions between Co and the carrier and better reducibility. Complete HCHO conversion was achieved over the Co-CD_{0.1}/Zr catalyst at 180 °C with 150 ppm HCHO and a GHSV of 30000 mL/(g·h) (Fig. 13). Wang et al. [100] prepared a 3D ordered mesoporous Co-Mn mixed oxide. This catalyst removed HCHO efficiently because of its large specific surface area and specific pore structure.

Table 2 shows that MnO_x-CeO₂ composite metal oxide catalysts [62,95,96] have good catalytic activities ($T_{50} < 100$ °C). This is because strong interactions between MnO_x and CeO₂ change the number of surface-active oxygen species and the active phase. Ma et al. [75] prepared 2D ordered mesoporous Co₃O₄-CeO₂. Under the same conditions, the HCHO conversion (20.3%) over 2D Co₃O₄ was higher than that (13.2%) over 2D Co₃O₄-CeO₂. This indicates that the addition Ce does not increase the catalytic activity, probably because a solid solution is not formed. Few composite metal oxide catalysts have been reported; therefore, syntheses of composite metal oxide catalysts with special morphologies for lower-temperature catalytic activity need to be developed.

4. Factors affecting HCHO oxidation activity

The catalytic activities of metal and transition-metal oxide catalytic systems in HCHO oxidation are affected by factors such as the preparation method, morphology and structure, specific surface area, active sites, low-temperature reducibility, and surface active oxygen species; these effects are inter-related. In addition, HCHO conversion by catalysts is influenced by experimental parameters such as the water vapor content, initial HCHO concentration, and space velocity.

4.1. Effect of preparation method

Catalysts or supports with different morphologies or higher surface areas can be obtained by using different preparation methods. The catalytic activity in HCHO oxidation varies de-

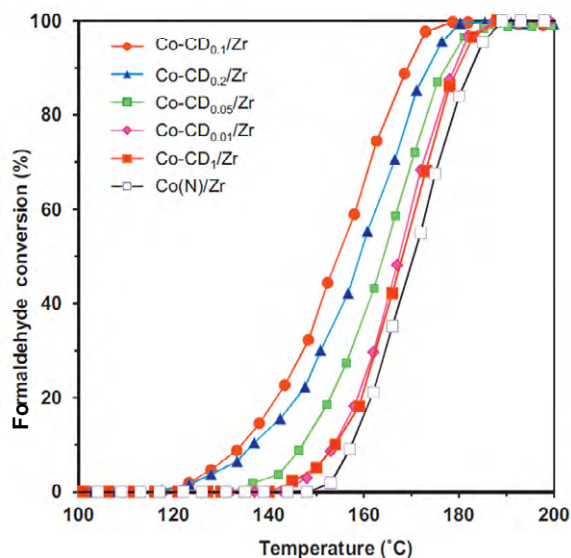


Fig. 13. HCHO conversions over various Co-CD_x/Zr catalysts [99].

pending on important factors such as active sites, surface-active oxygen species, and low-temperature reducibility. Changing the method used to prepare catalysts or supports is therefore an efficient way to obtain excellent catalytic activities for HCHO oxidation.

Zhou et al. [83] used KMnO₄ and oleic acid for the hydrothermal synthesis of MnO₂ samples with different crystalline structures (cryptomelane, birnessite, ramsdellite, and monoclinic crystals) and morphologies (nanosheets, nanospheres, and nanorods). They examined the effects of hydrothermal temperature, pH, and anion (PO₄³⁻, SO₄²⁻ and NO₃⁻) on the morphology and structure of MnO₂. The preparation method is shown in Fig. 14. The morphologies and structures of samples prepared hydrothermally at 80, 120, and 180 °C are δ-MnO₂ nanosheets, flower-like δ-MnO₂, and γ-MnOOH nanorods, respectively. The pH affects the size of cryptomelane α-MnO₂ nanorods. The samples prepared using PO₄³⁻, SO₄²⁻ and NO₃⁻ anions are flower-like δ-MnO₂, α-MnO₂ nanorods, and ramsdellite MnO₂, respectively. The results show that the crystalline structure of the catalyst significantly affects HCHO oxidation. Below 120 °C, the order of the catalytic activities in HCHO oxidation is cryptomelane MnO₂ > birnessite MnO₂ > ramsdellite MnO₂ > monoclinic MnOOH. The high activity of cryptomelane MnO₂ is attributed to the specific tunnel size of 0.46 × 0.46 nm², and large numbers of defects and surface hydroxyl groups. Tang et al. [95] prepared MnO_x-CeO₂ catalysts using sol-gel, coprecipitation, and modified coprecipitation methods. The MnO_x-CeO₂ sample prepared using the modified coprecipitation method gives the best catalytic performance in HCHO oxidation because it has more Mn⁴⁺ ions and surface lattice oxygen species. The formation of a solid-solution crystalline structure and improved reducibility also contribute to excellent oxidation activity. The Na-Pt/TiO₂ catalyst prepared by Zhang et al. [46] has the best activity in HCHO oxidation because of the addition of Na⁺ ions as auxiliaries during prepara-

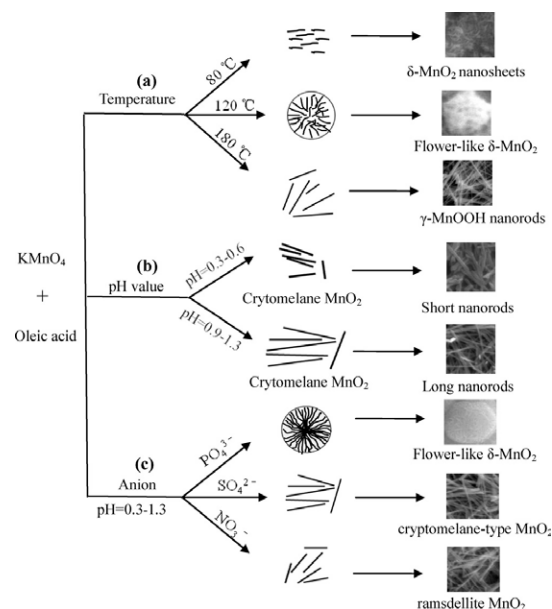


Fig. 14. Schematic diagram of growth of different manganese oxide nanostructures under various conditions [83].

tion. The addition of auxiliaries clearly increases the catalytic ability of Pt/TiO₂. HCHO at 600 ppm can be completely converted to CO₂ and H₂O at room temperature and a GHSV of 300000 h⁻¹ because of the large number of surface hydroxyl groups as surface-active oxygen species and better low-temperature reducibility. Our group [42] prepared mesoporous Co₃O₄ and bulk Co₃O₄ nanoparticles using hard template and precipitation methods, respectively. Mesoporous Co₃O₄ has better catalytic activity in HCHO oxidation, because the preparation method produces mesoporous Co₃O₄ with a special structure and morphology and an increased surface area; this enhances the active phase and low-temperature reducibility.

Table 1 and 2 confirm that the preparation method affects the catalytic activities of many catalysts. Transition-metal oxides with special morphologies and Ag or Au catalysts with such oxides as supports have promising low-temperature catalytic activities in HCHO oxidation because of the preparation methods used. However, catalyst preparation involves various factors such as choice of precipitant, the deposition rate, hydrothermal time and temperature, pH, template type, calcination temperature, auxiliaries, and choice of active components and supports. Much effort has been expended on the preparation of catalytic materials, but complete elimination of HCHO at room temperature has not yet been achieved. The experimental procedures for synthesizing materials is difficult and complex. One of the main aims in catalysis research is therefore the preparation of highly efficient catalysts using different methods.

4.2. Effects of morphology and structure

The morphologies and structures of catalysts depend on the preparation methods. Different morphologies and structure result in different surface areas, active phases or facets, reducibilities, and active oxygen species, and these affect the catalytic activities.

Our group [93,94] prepared 3D ordered mesoporous MnO₂, and α - and β -MnO₂ nanorod catalysts using hard template and hydrothermal methods, respectively. 3D MnO₂ consists of a β -MnO₂ crystalline phase corresponding to pyrolusite with a rutile structure. It has (211) and (332) low-angle diffraction peaks, which are characteristic of 3D ordered mesoporous structures with cubic symmetry (ia3d). The unit cell parameter of 3D MnO₂, calculated from the (211) diffraction, is 20.85 nm, and the unit cell parameter of the KIT-6 template is 21.63 nm. The two numbers are nearly equal, which confirms that 3D MnO₂ successfully replicates the 3D mesoporous structure of the KIT-6 template. Fig. 15 shows the ordered cubic (ia3d) mesoporous structure. The lattice dimension (19.66 nm), which was determined using TEM, matches the value calculated from the d_{211} spacing in the X-ray diffraction pattern. The electron diffraction pattern shows that 3D MnO₂ has a disordered polycrystalline wall. 3D MnO₂ also exposes the (110) and (101) crystal planes. α - and β -MnO₂ nanorods are non-porous materials (Fig. 15) with low surface areas and cryptomelane and pyrolusite, structures, respectively. 3D MnO₂ gives a better

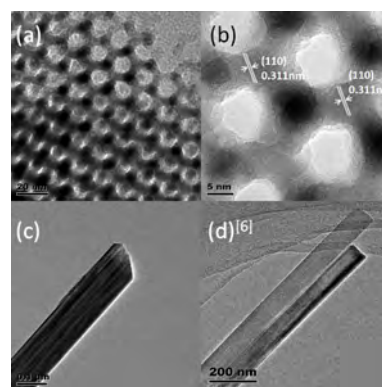


Fig. 15. TEM images of 3D MnO₂ (a, b), α -MnO₂ nanorods (c), and β -MnO₂ nanorods (d) [94].

catalytic performance, mainly because it has more surface Mn⁴⁺ ions as active sites and a higher surface area, as a result of its structure and morphology. Manganese oxides with pyrolusite, cryptomelane, and todorokite structures with different channel structures were also prepared (Fig. 16). Cryptomelane MnO₂ has the best catalytic activity, mainly because its channel size matches that of HCHO molecules, rather than because of its surface area and reducibility [84]. The order of the catalytic activities of these MnO₂ catalysts is cryptomelane (α -MnO₂) > todorokite (δ -MnO₂) > pyrolusite (β -MnO₂), because of their different crystalline structures. If the crystalline structure is unchanged but the morphology of pyrolusite MnO₂ is changed to mesoporous, the catalytic activity order changes to pyrolusite (3D mesoporous β -MnO₂) > cryptomelane (α -MnO₂ nanorods) > pyrolusite (β -MnO₂ nanorods).

The structure and morphology clearly affect the catalytic activity in HCHO oxidation. There are many papers on the effects of morphology and structure on the catalytic activities of materials such as nest-like MnO₂ [69], hollow K_xMnO₂ [88], OMS-2 [89,90], 3DOM CeO₂ [72], 3D Cr₂O₃ [92], 3D Co₃O₄ [42], and CeO₂ nanospheres [79].

4.3. Effect of specific surface area

A higher surface area exposes and disperses more noble-metal active sites and activates more HCHO molecules, and this can improve the catalytic activity in HCHO oxidation. This is why TiO₂, Al₂O₃, and molecular sieves are commonly used as supports for noble-metal catalysts. Relatively cheap Au or Ag loaded on metal oxide supports with high surface areas have

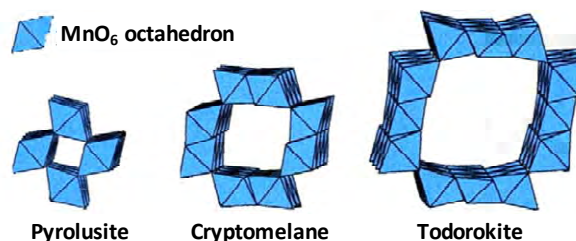


Fig. 16. Crystal structure models of three manganese oxides with different square tunnel sizes [84].

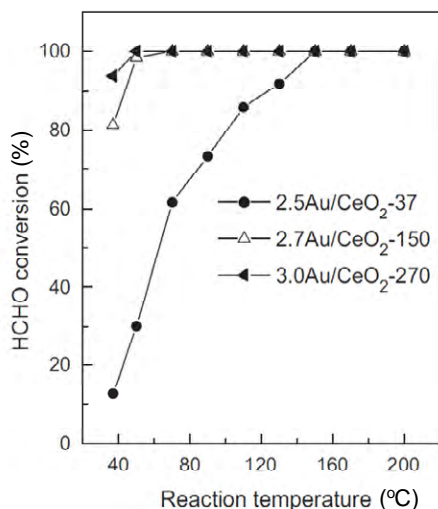


Fig. 17. Catalytic oxidation of HCHO over Au/CeO₂ catalysts [65].

good potential as catalysts. Li et al. [65] reported that Ag/CeO₂ catalysts with different surface areas showed different catalytic activities in HCHO oxidation (Fig. 17). A higher surface area favors the formation of Au species with high oxidation states and Au_xCe_{1-x}O_{2-δ} solid solutions.

Higher surface areas can also improve the catalytic activities of metal oxide catalysts by enhancing factors such as the reducibility, active phase, and oxygen species. Dai's group [92] prepared 3D mesoporous Cr₂O₃ with high surface areas (Table 3). 3D Cr₂O₃ has better catalytic activity than bulk Cr₂O₃, which has a smaller surface area (5 m²/g). Zhang et al. [72] prepared 3DOM CeO₂. The catalytic activity of 3DOM CeO₂-80 in HCHO oxidation is better than that of 3DOM CeO₂-100, because 3DOM CeO₂-80 has a higher surface area. Our group reported that 3D Co₃O₄ [42], 3D MnO₂ [94], and CeO₂ nanosphere [79] catalysts gave good catalytic performances because of their low-temperature reducibilities and large numbers of metal cations, resulting from their high surface areas. Some studies of oxidation of other VOCs have also shown that a higher surface area improves the catalytic activity [101,102].

However, the surface area is not the decisive factor in catalytic oxidation. Sometimes a higher surface area does not result in a better catalytic performance. For instance, Yu et al. [69] prepared MnO₂ catalysts with higher surface areas. Specific surface areas of cocoon-like MnO₂, sea-urchin-like MnO₂, and nest-like MnO₂ are 247.6, 62.3 and 56.9 m²/g, respectively. Fig. 18 shows that nest-like MnO₂ has the smallest surface area and

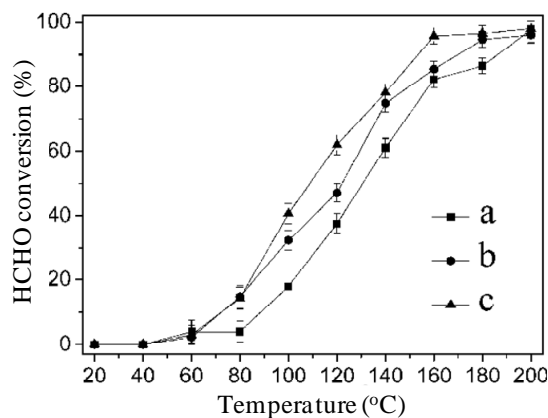


Fig. 18. Catalytic performances in HCHO oxidation of (a) cocoon-like MnO₂, (b) sea-urchin-like MnO₂, and (c) nest-like MnO₂ [69].

the best catalytic activity; this is because the channels of width 0.6 nm are suitable for adsorption of HCHO molecules. Although cocoon-like MnO₂ has the highest surface area, its low crystallinity prevents the formation of micropores.

4.4. Effect of active sites

The active sites are one of the decisive factors in determining the catalytic activity. A larger number of active sites can directly improve the oxidation abilities of catalysts, but this is a complex and abstract topic. In HCHO oxidation, noble metals (Pt, Pd, Au, and Ag) often provide better active sites. Most catalysts with Pt and Pd as active sites have excellent catalytic performances in the oxidation of HCHO and other VOCs because of the stronger ability of these metal atoms to activate O–O and C–H bonds [103,104]. The active sites of transition-metal oxide catalyst are usually provided by metal ions with high oxidation states. The activation ability of a noble metal is much stronger than those of high-valence transition-metal cations such as Mn⁴⁺, Co³⁺, and Cr⁶⁺. This is why addition of a noble metal can result in complete HCHO conversion at lower temperatures under normal circumstances.

In the Refs. [52,53,70,78,93], active sites are often defined as the number of noble-metal atoms or metal cations with high valence states on the catalyst surface. Generally, dispersion, which is related to the noble-metal particle size and loading, determines the number of active sites on a supported noble-metal catalyst. For example, Huang et al. [52] reported that a PdO–DP catalyst achieved higher HCHO conversion than a PdO–IMP catalyst, because of its higher Pd dispersion, which results in more active sites. The Pd–DP–NaBH₄ catalyst has a higher TOF because of its higher Pd dispersion, Pd metallic state, and smaller particle size. Huang et al. [70] prepared a catalyst with stable single-atom Ag chains in HMO tunnels. Ag atoms replace K⁺ ions in the channel structure of Mn octahedral sieves. The single Ag atoms at the openings of the tunnels of Ag–HMO nanorods are defined as active sites. The Ag–HMO catalyst has a better catalytic activity than a Ag/HMO catalyst with supported Ag nanoparticles, because the higher Ag dispersion increases the number of active sites. On transi-

Table 3

Textural properties of KIT-6 and Cr₂O₃ catalysts [92].

Sample	Surface area (m ² /g)	Average pore diameter (nm)	Pore volume (cm ³ /g)
KIT-6	790	6.1	0.95
bulk-Cr	5	—	—
meso-Cr-200	91	7.7	0.13
meso-Cr-300	98	7.6	0.14
meso-Cr-400	124	7.9	0.21
meso-Cr'-400	69	8.2	0.12
meso-Cr-500	109	8.9	0.16

tion-metal oxide catalysts, surface metal cations with high valence states determine the number of active sites. Tang et al. [95] reported a $\text{MnO}_x\text{-CeO}_2$ sample that had good catalytic activity because of the large number of surface Mn^{4+} ions and lattice oxygen species. Our group reported that more metal cations clearly improved the HCHO oxidation activities on 3D Co_3O_4 [42] and 3D MnO_2 [94] catalysts.

4.5. Effect of low-temperature reducibility

Low-temperature reducibility is an important factor in oxidation reactions. Better reducibility means that oxygen species are easily activated or can easily migrate to the catalyst surface. It has been reported that better catalytic activity is related to lower-temperature reducibility. He's group reported that the reducibility of a Na-Pt/TiO_2 catalyst correlated with its activity [46]. Fig. 19 shows that Na addition shifts the reduction peak to lower temperature. Tang's group prepared $\text{Ag/MnO}_x\text{-CeO}_2$ [63], which has good catalytic activity because of its low-temperature reducibility. $\text{Ag/MnO}_x\text{-CeO}_2$ shows a reduction peak at 293 °C. The presence of Ag shifts the reduction peak to lower temperature compared with that for $\text{MnO}_x\text{-CeO}_2$, because of interactions between Ag and $\text{MnO}_x\text{-CeO}_2$. Dai's group reported that 3D Cr_2O_3 calcined at 400 °C had the best catalytic activity in HCHO oxidation among a group of Cr catalysts calcined at different temperatures [92]. The initial H_2 consumption rate was used to evaluate the catalyst reducibilities. The order of the initial H_2 consumption rates is $\text{Cr-400} > \text{Cr-300} > \text{Cr-500} > \text{Cr-200} > \text{bulk Cr}$, which indicates that 3D Cr-400 has the best reducibility, which correlates with the catalytic activities. Our group also reported that a $\text{K-Ag/Co}_3\text{O}_4$ catalyst has the best activity and low-temperature reducibility of all samples examined [78]. The addition of K^+ ions shifts the reduction peak to lower temperature.

4.6. Effect of surface oxygen species

A large number of surface oxygen species improves the catalytic activity. The adsorption, activation, and migration of oxygen during the oxidation reaction is complex. The consump-

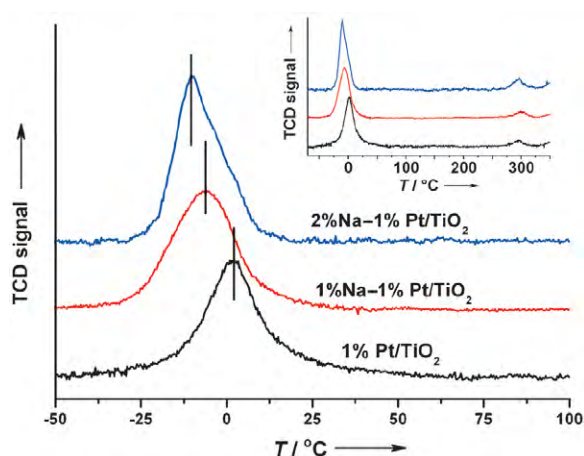


Fig. 19. H_2 -temperature-programmed reduction profiles of x wt% Na-1\% Pt/TiO_2 ($x = 0, 1, \text{ and } 2$) [46].

tion and supply of oxygen species occur continuously on the catalyst surface. Generally, a catalyst with abundant surface oxygen species has better activity than one with few such species in the catalytic oxidation of HCHO.

Our group loaded Ag nanoparticles on 3D Co_3O_4 [78]. $\text{Ag/Co}_3\text{O}_4$ has more surface lattice oxygen species because of the presence of Ag, and has better catalytic activity than 3D Co_3O_4 . The addition of K^+ ions to $\text{Ag/Co}_3\text{O}_4$ gave $\text{K-Ag/Co}_3\text{O}_4$ has a large number of surface hydroxyls as surface adsorbed oxygen species, because of the presence of K^+ ions, and shows better activity than $\text{Ag/Co}_3\text{O}_4$. Surface adsorption and lattice oxygen species on $\text{K-Ag/Co}_3\text{O}_4$ are involved in the activation and migration of oxygen, and this increases the oxidation activity in HCHO. Zhang et al. [46] added Na^+ ions to Pt/TiO_2 , which provided abundant surface hydroxyls on the Na-Pt/TiO_2 catalyst. Na-Pt/TiO_2 shows the best activity in HCHO oxidation. Surface hydroxyls as active oxygen species directly change the reaction route of HCHO oxidation. Different preparation methods lead to different surface oxygen species. Large amounts of surface chemisorbed oxygen form on Ag/CeO_2 [79] and 3D Co_3O_4 [42], and this improves their catalytic activity in HCHO oxidation.

4.7. Effects of experimental parameters

Different experimental parameters such as water vapor content, initial HCHO concentration, and space velocity, can lead to different HCHO conversions. Generally, catalytic conversion of HCHO decreases with increasing initial HCHO concentration and GHSV. Huang et al. [52] examined the effect of initial HCHO concentration in the range 5–30 ppm. The steady conversions of HCHO were 100% at 5 ppm, 99.1% at 10 ppm, 98.2% at 20 ppm, and 95.8% at 30 ppm. As anticipated, the HCHO removal efficiency decreased with increasing initial HCHO concentration. The effect of GHSV on HCHO oxidation was investigated using 0.1% Pt-TiO_2 in the range 40000–240000 h^{-1} . The steady conversions of HCHO were 100% at 40000 h^{-1} , 99.1% at 80000 h^{-1} , 97.8% at 160000 h^{-1} , and 90.5% at 240000 h^{-1} . The HCHO conversion decreased with increasing GHSV. Tang et al. [62] investigated the effect of HCHO concentration. They achieved 100% conversion of HCHO at HCHO concentrations less than 100 ppm; the conversion decreased slightly with increasing HCHO concentration. The HCHO conversion was 50% at an HCHO concentration of 580 ppm. The HCHO conversion decreased with increasing feed concentration. Xia et al. [92] examined the effects of GHSV on HCHO, acetone, and methanol oxidation in the range 10000–60000 h^{-1} . The results confirm that conversion over 3D Cr_2O_3 decreased with increasing of GHSV.

For the catalytic oxidation of other VOCs such as ethanol [93,105], CH_4 [101], and toluene [106], the addition of water vapor shifts complete conversion to higher temperatures. The VOC conversion decreases with increasing water vapor content. However, the presence of water vapor improves HCHO conversion. Huang et al. [52] studied the effect of moisture. HCHO oxidation was promoted by water vapor up to 50% humidity. Nearly 100% HCHO conversion was achieved at humidities of

25% and 50%, but the conversion was only 45.2% at the stable stage at 0% humidity. The HCHO conversion decreased slightly at humidities higher than 50% because of coverage of active centers by water, but the removal efficiency was still as high as 95.6% at 97.5% humidity. The presence of moisture did not inhibit, but enhanced, HCHO oxidation at room temperature.

The catalytic activities in HCHO oxidation of different catalysts were compared under the same conditions. Changes in the GHSV and initial HCHO concentration hinder comparison of the oxidation activities of various catalysts. Normalized rates, i.e., mol/(m²·h) or mol/(m²·s), and TOFs (s⁻¹ or h⁻¹) should therefore be used to calculate HCHO oxidation activities. In real situations, water vapor is often present in indoor environments and vehicle exhausts. It is therefore necessary to examine the effect of moisture on catalytic activity.

5. Reaction mechanism

Research on the mechanism of HCHO oxidation is a sophisticated process. Several mechanisms have been proposed based on the Mars–van Krevelen mechanism. He's group [45] reported the reaction mechanism on TiO₂-supported noble-metals catalysts (Fig. 20). Dioxymethylene, formate, and adsorbed CO are important reaction intermediates in HCHO oxidation. The decomposition of surface formate species to adsorbed CO on the catalyst is the rate-determining step for catalytic oxidation of HCHO. HCHO is oxidized to surface dioxymethylene species, and then formate species. The surface formate species decompose to adsorbed CO species and H₂O, and then the CO species react with O₂ to produce gas-phase CO₂. Pt/TiO₂ shows high activity in HCHO oxidation because decomposition of formate species is easier on this catalyst than on supported catalysts containing Rh, Pd, and Au. The same group reported that the reaction mechanism over a Na–Pt/TiO₂ catalyst differed from that on a Pt/TiO₂ catalyst [46]. Na–Pt/TiO₂ has the best catalytic activity in HCHO oxidation because of the surface hydroxyl groups formed by Na⁺ ions; the reaction mechanism differs from that over Pt/TiO₂ because of the addition of Na. The HCHO oxidation reaction on Na-free Pt/TiO₂ follows the formate decomposition route (HCHO → CHOO⁻ → CO → CO₂), with formate decomposition to CO being the rate-determining step. However, HCHO oxidation over 2% Na–1% Pt/TiO₂ follows a different pathway, HCHO → CHOO⁻ + •OH → CO₂ + H₂O. The reaction between surface hydroxyls and formate is easier than decomposition of formate to CO followed by CO oxidation. The process in which formate species on the catalyst surface directly react with surface hydroxyl groups to form CO₂ and H₂O becomes the rate-determining step. Nie et al. [47] reported the

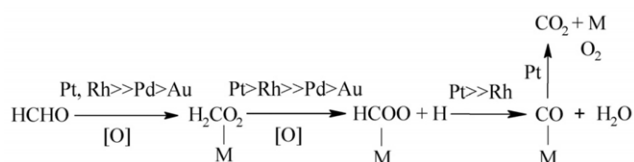


Fig. 20. Reaction scheme for catalytic oxidation of HCHO on TiO₂-supported Pt, Rh, Pd, and Au catalysts [45].

same reaction mechanism for HCHO oxidation on the Na–Pt/TiO₂ catalyst.

Our group [78] reported the reaction mechanism for HCHO oxidation on a 3D K–Ag/Co₃O₄ catalyst (Fig. 21). K–Ag/Co₃O₄ has a large number of Ag (111) crystal facets, surface lattice oxygen (O²⁻) species, and Co³⁺ cations because of the addition of K⁺ ions; these are all involved in the oxidation reaction. K⁺ ion addition changes the reaction route of HCHO oxidation on 3D K–Ag/Co₃O₄ catalyst, as in the case of 2% Na–1%Pt/TiO₂ catalyst [46]. Research shows that more Co³⁺ cations can increase the oxygen vacancy density; these vacancies result from anionic structural defects. The oxygen vacancies directly participate in the adsorption, activation, and migration of oxygen. The Ag (111) planes are active faces in HCHO oxidation and can activate the O²⁻ species of 3D Co₃O₄. The O²⁻ species can also improve the reactivity of the Ag (111) surfaces, enhance the breakage of H₂, O₂, and NO bonds, and strengthen the bonding of H, O, N, and C atoms to the Ag (111) surface. In the reaction, the active O²⁻ species around Ag are directly depleted and replenished by the Co₃O₄ support, which acts as an oxygen reservoir. The activation and migration of oxygen species at the oxygen vacancies depend on the Co³⁺/Co²⁺ and Ag⁺/Ag⁰ redox cycles after the O²⁻ species are consumed (Fig. 21, yellow box). The redox cycle is possibly the same as the Mn⁴⁺/Mn³⁺ and Ce⁴⁺/Ce³⁺ redox cycles reported by Tang et al. [62]. The increase in the number of Co³⁺ ions favors the formation of oxygen vacancies, which can enhance the Co³⁺/Co²⁺ and Ag⁺/Ag⁰ redox cycles. In addition, the addition of K⁺ ions results in the presence on the K–Ag/Co₃O₄ catalyst surface of adsorbed oxygen species, in the form of hydroxyl species. Surface hydroxyl species play a critical role in the reaction path of HCHO oxidation. A surface hydroxyl can immediately react with formate species on the K–Ag/Co₃O₄ surface to form a molecule of CO₂ and H₂O. This is similar to the reaction path for the Na–Pt/TiO₂ catalyst [46]. The difference is that O²⁻ species at the perimeter of Ag in K–Ag/Co₃O₄ participate in HCHO oxidation because of strong interactions between Ag with Co and anionic lattice defects. The TOFs of K–Ag/Co₃O₄, especially 1.7% K–Ag/Co₃O₄, are much higher than that of Ag/Co₃O₄. It is concluded that at low temperature (< 80 °C), the catalytic activity of K–Ag/Co₃O₄ in HCHO oxidation largely depends on surface •OH species at the perimeters of Ag (111) facets; at higher temperatures (>80 °C), the surface •OH species are consumed and replaced quickly, and their supply relies on the migration of O²⁻ species from the 3D Co₃O₄ support. The reaction pathway of HCHO oxidation on K–Ag/Co₃O₄ is therefore HCHO → CHOO⁻ + •OH → CO₂ + H₂O. For Ag/Co₃O₄, the reaction pathway is HCHO → CHOO⁻ →

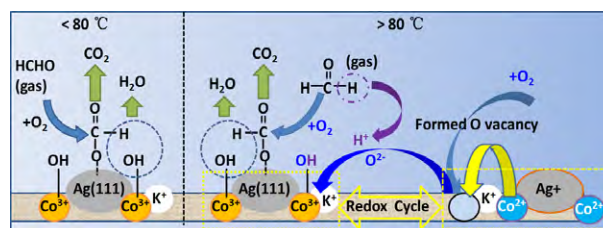


Fig. 21. Reaction pathway on K–Ag/Co₃O₄ catalyst [78].

$\text{CO} + \text{O}^* \rightarrow \text{CO}_2$. The O^{2-} species play an important role on the oxidation reaction and active O^* species are often involved in complex migration through oxygen vacancies. The TOFs of $\text{Ag}/\text{Co}_3\text{O}_4$ show that the catalytic activity depends on the O^{2-} species around Ag nanoparticles at low temperature ($<90^\circ\text{C}$), and on the O^{2-} species at the perimeter of Ag, which migrate from the 3D Co_3O_4 support at higher temperatures ($>90^\circ\text{C}$).

Liu et al. [73] reported the mechanism of HCHO oxidation on a 3DOM Au/CeO_2 catalyst (Fig. 22). HCHO oxidation occurs via two processes, catalyzed by ionic Au^{3+} and metallic Au^0 , respectively; Au^{3+} shows higher catalytic activity. The CeO_2 support in contact with Au^{3+} may be partly reduced to Ce_2O_3 when Au^{3+} ions are formed on the surface of the 3DOM Au/CeO_2 catalyst. After adsorption of HCHO molecules on the surface of the CeO_2 support, active oxygen may be transferred from Au_2O_3 to HCHO to form HCOOH and Au^0 . HCOOH is then converted to formate through interactions with the CeO_2 support, accompanied by loss of $\cdot\text{H}$ to form H_2O with free $\cdot\text{OH}$ adsorbed on the surface of the CeO_2 support. Incomplete oxidation of HCOOH also occurs, which enables conversion of HCOOH to carbonate and hydrocarbonate. H_2O is generated when the lost $\cdot\text{H}$ interacts with free $\cdot\text{OH}$. HCHO is converted to CO_2 and H_2O via this cycle. The Au^{3+} in the 3DOM Au/CeO_2 catalyst determines the efficiency of the HCHO conversion. HCHO oxidation catalyzed by metallic Au^0 via another process is also involved, but is not the dominant process. After HCHO adsorption on the CeO_2 support, active oxygen is transferred to HCHO to form HCOOH, and then HCOOH is converted to CO_2 and H_2O , completing the oxidation process. Incomplete oxidation occurs simultaneously to form carbonate and hydrocarbonate, which may deactivate the 3DOM Au/CeO_2 catalyst. In the HCHO oxidation process, there is a balance between HCOOH adsorption and desorption, to form formate on the CeO_2 support. HCOOH can therefore be converted to CO_2 and H_2O through complete oxidation, and formate can be converted to carbonate and hydrocarbonate via incomplete oxidation; these are deposited on the surface of the CeO_2 support and deactivate the catalyst. Blockage of the active sites on 3DOM Au/CeO_2 by carbonate and hydrocarbonate is difficult, because of the macroporous structure of the catalyst.

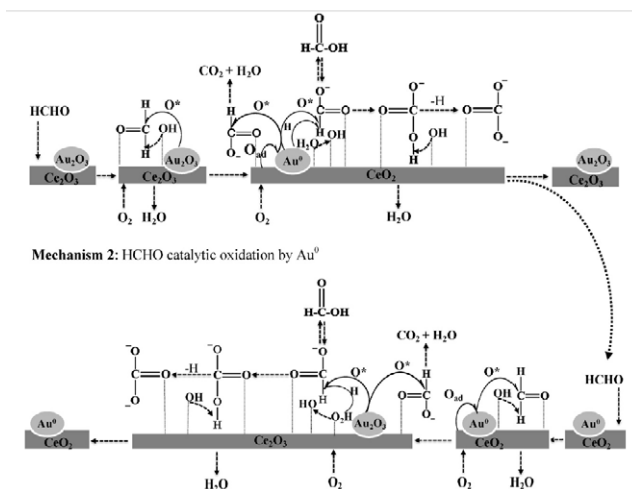


Fig. 22. Mechanism of HCHO oxidation on 3DOM Au/CeO_2 catalyst [73].

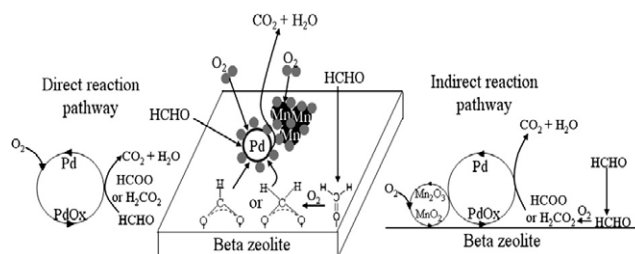


Fig. 23. HCHO oxidation pathway over 0.25 Pd/20 Mn/Beta catalyst [54].

According to the literature, the addition of Na^+ or K^+ ions, which results in formation of hydroxyl oxygen species on the catalyst surface, can change the reaction route and increase the catalytic activity. This can be used to help design methods for catalyst preparation. Perhaps the HCHO oxidation activities of other supported noble-metal catalysts could be increased by alkali metal addition. In HCHO oxidation, abundant surface oxygen species participate in the oxidation reaction, and this enhances the catalytic activity. Surface-active oxygen species depend on the redox cycles of high- and low-valent states of metal cations, and this directly affects the adsorption, activation, and migration of oxygen species. Park et al. [54] reported indirect and direct reaction pathways over a 0.25 Pd/20 Mn/Beta catalyst; these are two types of redox cycle, and the cycle depends on whether Mn cations participate in the reaction at a given temperature (Fig. 23). Tang et al. [62,63] proposed two redox cycles for HCHO oxidation over $\text{Pt}/\text{MnO}_x\text{-CeO}_2$ and $\text{Ag}/\text{MnO}_x\text{-CeO}_2$ catalysts to explain the formation of active oxygen; these are displayed in Fig. 24. HCHO oxidation over different catalysts may involve different reaction mechanisms, probably because different active oxygen species and sites can form different reaction intermediates. Formate species are important reaction intermediates in HCHO oxidation; they are present on all reported catalysts, and can produce different intermediates on different catalysts. There are three processes. (1) Formate species can decompose to adsorbed CO followed by CO oxidation on the surfaces of catalysts such as Pt/TiO_2 [45] and $\text{Ag}/\text{Co}_3\text{O}_4$ [78]. (2) Formate species can react with surface hydroxyls to form CO_2 and H_2O directly on the surfaces of catalysts such as $\text{Na-Pt}/\text{TiO}_2$ [46] and $\text{K-Ag}/\text{Co}_3\text{O}_4$ [78]. (3) Formate species can form carbonate and then decompose to CO_2 on the surfaces of catalysts such as 3DOM Au/CeO_2 [73] and 2D $\text{Au}/\text{Co}_3\text{O}_4\text{-CeO}_2$. The mechanism of HCHO oxidation on a 2D $\text{Au}/\text{Co}_3\text{O}_4\text{-CeO}_2$ catalyst was reported by Ma et al. [75]. As shown in Fig. 25, HCHO is oxidized to formate species, which

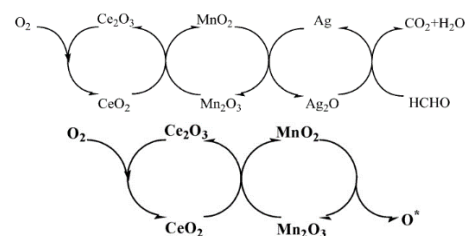


Fig. 24. Redox cycles in HCHO oxidation over $\text{MnO}_x\text{-CeO}_2$ and $\text{Ag}/\text{MnO}_x\text{-CeO}_2$ [62,63].

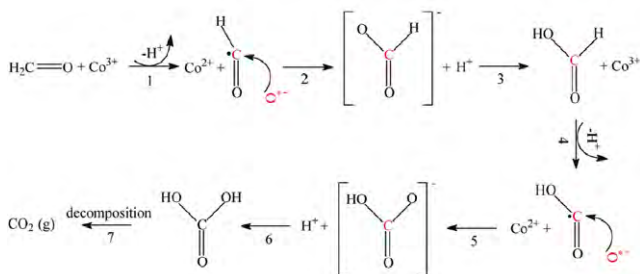


Fig. 25. Reaction route for HCHO oxidation over mesoporous Au/Co₃O₄-CeO₂ [75].

form carbonate. The carbonate decomposes to CO₂ and OH⁻. Further studies are needed to enable a deeper understanding of the mechanism of HCHO oxidation. The reaction mechanisms over more catalysts need to be clarified to obtain a more comprehensive understanding.

6. Results and outlook

HCHO is a carcinogenic and teratogenic substance, and has strong photochemical activity. It is emitted during the production of textiles, agrochemicals, sheet materials, and fine chemicals, from motor vehicle exhausts, and from various indoor decorating materials. HCHO removal is necessary to protect human health and the atmospheric environment. The removal of HCHO through catalytic oxidation is a more promising technique than adsorption methods. The key to this technique is the development of suitable catalysts. Catalytic materials for HCHO oxidation can be divided into noble-metal and transition-metal oxide systems. Noble-metal catalysts are generally prepared by loading noble metals (Pt, Pd, Au, and Ag) on various supports. Supports can be classified as common supports, traditional metal oxide supports, and metal oxide support with special morphologies. The common supports used in HCHO oxidation are usually materials such as SiO₂, Al₂O₃, TiO₂, and molecular sieves. These have large surface areas, and this is conducive to the exposure of active sites and the adsorption and diffusion of reactants and products, and can enhance the synergistic effect between the support and the active component. The catalytic HCHO oxidation activities of different noble-metal catalysts loaded on common supports decrease in the following order: Pt > Pd > Rh > Au > Ag. This type of catalyst is suitable for applications in indoor environments and factories, and for vehicle exhausts, except in terms of cost and thermostability. Na-Pt/TiO₂ [46], which is used in air purifiers, is the best catalyst for HCHO removal, followed by Pt/TiO₂ and Pd/TiO₂ [53]. The use of different supports with the same active components directly affects the activities of catalysts for HCHO oxidation. Precious metals have been loaded on metal oxide supports with the aim of obtaining the advantages of both noble-metal and metal oxide catalysts; such catalysts have better low-temperature oxidation activities and thermostabilities because of the interactions between the metal and the support. Metal oxide supports such as CeO₂, Fe₂O₃, Co₃O₄, and MnO₂, or their composites, prepared by conventional precipitation, coprecipitation, or sol-gel methods, used in HCHO oxidation are defined as tra-

ditional metal oxide supports. This type of supported Pt catalyst has excellent catalytic activity (*T*₅₀) at room temperature; examples are Pt/MnO_x-CeO₂ [62] and Pt/Fe₂O₃ [67]. Although supported Pt catalysts are promising for various applications, they are too expensive and their industrial production and use are limited. If the Pt loading is decreased to reduce the production cost, the reaction performance of the catalyst may be compromised. Some catalysts with traditional metal oxide supports, such as Au/CeO₂ [65], Ag/MnO_x-CeO₂ and Ag/CeO₂ [63], have better development potential, because of the strong interactions between the noble metal and the support. The choice of support for HCHO oxidation catalysts is important. The trend is not to choose Pt or Pd as the active components of catalysts of HCHO removal, and supported Au or Ag catalysts may provide suitable alternatives. Traditional metal oxide supports can be modified by using different preparation methods. Metal oxides with special morphologies and structures, such as nanorods, nanospheres, mesopores, and macropores, are mainly prepared using hydrothermal and hard template methods. Such materials may provide new supports with catalytic activities better than those of conventional bulk metal oxides prepared using precipitation methods. Few Pt catalysts have been produced using metal oxide supports with special morphologies, because 2% Na-1% Pt/TiO₂ has become the benchmark for supported Pt catalysts in air purification [46]. More attention has been paid to catalysts consisting of Ag and Au loaded on metal oxide supports with special morphologies. These catalysts, e.g., mesoporous 3DOM Au/CeO₂-Co₃O₄ [74], 2D Au/Co₃O₄-CeO₂, 2D Au/Co₃O₄ [75], and 3D K-Ag/Co₃O₄ [78], have excellent catalytic activities in room-temperature HCHO oxidation (*T*₅₀ = room temperature) and have good potential applications.

Transition-metal oxide catalysts have cheap and plentiful sources, and have been widely studied. Single transition-metal oxide catalysts such as MnO₂ nanorods, cryptomelane nanospheres, and mesoporous MnO₂, Co₃O₄, and Cr₂O₃ have good catalytic activities in HCHO oxidation, and their *T*₅₀ and *T*₁₀₀ HCHO conversions are less than or equal to 110 and 140 °C, respectively. Their catalytic activities are superior to those of traditional metal oxide catalysts synthesized using precipitation methods, because of their special morphologies and structures, higher surface areas, and other factors that improve the catalytic activity. Single transition-metal oxide catalysts with special morphologies have good application prospects because they are cheap and give better catalytic performances. Some metal elements (such as Ce, Sn, Cu, and Zr) can be doped into MnO_x and Co₃O₄ to prepare composite metal oxides when a single metal oxide does not give a good catalytic performance. The composite metal oxide catalyst MnO_x-CeO₂ [95, 96] has excellent catalytic activity (*T*₅₀ < 100 °C) because the strong interactions between MnO_x and CeO₂ change the number of surface-active oxygen species and the active phase. Few composite metal oxide catalysts have been reported; therefore, the development of composite metal oxide catalysts with special morphologies for lower-temperature catalytic activities is an area for future exploration. The use of different preparation methods may provide single transition-metal oxides or compo-

site oxide catalysts that can be used as substitutes for noble-metal catalysts, including Au and Ag, for VOC oxidation.

The catalytic activity in HCHO oxidation is affected by factors such as the preparation method, morphology and structure, specific surface area, active sites, low-temperature reducibility, and surface-active oxygen species; these factors are related to each other. Different preparation methods can provide various catalysts or supports with different morphologies or higher surface areas, which may further change some important factors such as the active sites, surface-active oxygen species, and low-temperature reducibility of the catalysts. Changing the methods used to prepare catalysts or supports is therefore an efficient way to obtain excellent catalytic activities in HCHO oxidation. Transition-metal oxides with special morphologies and their supported Ag or Au catalysts have promising low-temperature catalytic activities in HCHO oxidation because of the special preparation methods used. Catalytic HCHO conversion is also influenced by experimental parameters such as water vapor content, initial HCHO concentration, and GHSV. The activities of various HCHO oxidation catalysts were compared under the same condition. Changes in the GHSV and initial HCHO concentration are not useful in comparison of the oxidation activities of different catalysts. Normalized rates ($\text{mol}/(\text{m}\cdot\text{h})$ or $\text{mol}/(\text{m}\cdot\text{s})$) and TOFs (s^{-1} or h^{-1}) should be used to express the activity in HCHO oxidation. In real situations, water vapor is often present in indoor environments and vehicle exhausts. It is therefore necessary to examine the effects of moisture on catalytic activity.

The development of effective and low-cost catalysts for HCHO oxidation at low temperatures, even room temperature, is still an important challenge. Catalyst preparation involves various factors such as choice of precipitant, deposition rate, hydrothermal time and temperature, pH, templates, calcination temperature, auxiliaries, and choice of active components and supports. Much time has been spent on the preparation of catalytic materials, but catalysts with improved oxidation abilities are still needed. The experimental processes involved in synthesizing materials are difficult and complex. Compared with noble-metal catalysts, transition-metal oxides have better high-temperature catalytic activities, and it is very difficult to completely convert HCHO at room temperature. To control some of the factors influencing catalytic activity, such as struc-

ture, morphology, and specific surface area, metal oxides with rod-like, spherical, and porous structures, with high surface areas, have been prepared using various synthetic methods to improve the catalytic performances in HCHO oxidation. For example, the low-temperature catalytic activities of 3D Cr_2O_3 and 3D Co_3O_4 , and MnO_2 nanorods and nanospheres are better than those of traditional bulk Cr_2O_3 , Co_3O_4 , and MnO_x . However, there is still a need for catalysts with special morphologies that can completely convert HCHO at low temperatures, even room temperature. Catalysts with carriers with different morphologies are promising for achieving complete HCHO conversion at low temperatures. A potential catalyst can be prepared by loading Pt or Pd on the support surface. However, a balance needs to be struck between the cost of precious metals and catalytic performance. Ag and Au are relatively cheap precious metals. The synthesis of catalysts consisting of Ag or Au loaded on metal oxide supports with special morphologies may be a future trend in developing catalysts supported on transition-metal oxides for complete conversion of HCHO at room temperature.

Research on the mechanism of HCHO oxidation is a sophisticated process; few mechanisms have been reported in the literature. To understand HCHO oxidation in depth, it is necessary to study the reaction mechanism further. The reaction mechanisms over more catalysts need to be reported in the future to obtain a more comprehensive understanding of HCHO oxidation. The structure–activity relationships of the catalysts also need to be further researched using various physical and chemical characterization techniques, especially in situ Raman, infrared, and near-edge X-ray absorption fine structure spectroscopies. The preparation and development of new nanocatalysts with various morphologies and structures will become a research trend in the future. Such materials can be used in the catalytic oxidation of HCHO and the catalytic oxidation of benzene series or other VOCs, and could provide techniques for decreasing VOC discharges from vehicle exhausts and industrial processes. The removal of VOCs helps to decrease of $\text{PM}_{2.5}$ levels and to improve the atmospheric air quality.

Acknowledgements

This study was supported by the State Environmental Pro-

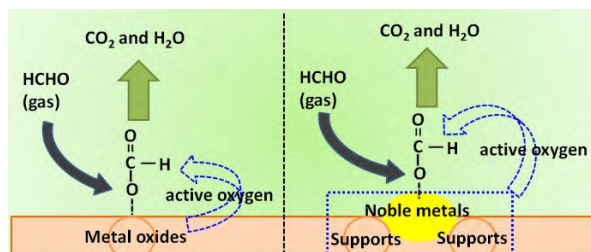
Graphical Abstract

Chin. J. Catal., 2016, 37: 102–122 doi: 10.1016/S1872-2067(15)61007-5

Progress in research on catalysts for catalytic oxidation of formaldehyde

Bingyang Bai*, Qi Qiao, Junhua Li*, Jiming Hao
Chinese Research Academy of Environmental Sciences;
Tsinghua University

This paper reviews progress in research on precious-metal and transition-metal oxide catalyst systems for HCHO oxidation. The oxidation properties, factors influencing the catalytic activity, and reaction mechanisms are discussed, and future development directions and research hotspots are considered.



tection Key Laboratory of Sources and Control of Air Pollution Complex, and also supported by the State Key Laboratory of Environmental Criteria and Risk Assessment, Chinese Research Academy of Environmental Science.

References

- [1] T. Salthammer, S. Mentese, R. Marutzky, *Chem. Rev.*, **2010**, 110, 2536.
- [2] M. Hakim, Y. Y. Broza, O. Barash, N. Peled, M. Phillips, A. Amann, H. Haick, *Chem. Rev.*, **2012**, 112, 5949.
- [3] O. S. Wenger, *Chem. Rev.*, **2013**, 113, 3686.
- [4] R. J. Avery, *Environ. Sci. Technol.*, **2006**, 40, 4845.
- [5] S. P. Chen, T. H. Liu, T. F. Chen, C. F. Ouyang, J. L. Wang, J. S. Chang, *Environ. Sci. Technol.*, **2010**, 44, 4635.
- [6] C. Domeño, Á. Rodríguez-Lafuente, J. Martos, R. Bilbao, C. Nerín, *Environ. Sci. Technol.*, **2010**, 44, 2585.
- [7] D. J. Luecken, M. R. Mebust, *Environ. Sci. Technol.*, **2008**, 42, 1615.
- [8] B. Cardoso, A. S. Mestre, A. P. Carvalho, J. Pires, *Ind. Eng. Chem. Res.*, **2008**, 47, 5841.
- [9] Y. C. Chiang, P. C. Chiang, C. P. Huang, *Carbon*, **2001**, 39, 523.
- [10] S. Brosillon, M. H. Manero, J. N. Foussard, *Environ. Sci. Technol.*, **2001**, 35, 3571.
- [11] I. Ushiki, M. Ota, Y. Sato, H. Inomata, *Fluid Phase Equilib.*, **2015**, 403, 78.
- [12] N. Yao, K. L. Yeung, *Chem. Eng. J.*, **2011**, 167, 13.
- [13] R. Tejasvi, M. Sharma, K. Upadhyay, *Chem. Eng. J.*, **2015**, 262, 875.
- [14] M. Hussain, N. Russo, G. Saracco, *Chem. Eng. J.*, **2011**, 166, 138.
- [15] F. Moulis, J. Krýsa, *Catal. Today*, **2013**, 209, 153.
- [16] F. Wang, H. X. Dai, J. G. Deng, G. M. Bai, K. M. Ji, Y. X. Liu, *Environ. Sci. Technol.*, **2012**, 46, 4034.
- [17] J. G. Deng, L. Zhang, H. X. Dai, Y. S. Xia, H. Y. Jiang, H. Zhang, H. He, *J. Phys. Chem. C*, **2010**, 114, 2694.
- [18] Q. Ye, J. S. Zhao, F. F. Huo, D. Wang, S. Y. Cheng, T. F. Kang, H. X. Dai, *Microporous Mesoporous Mater.*, **2013**, 172, 20.
- [19] H. Arandiyán, H. X. Dai, J. G. Deng, Y. Wang, H. Y. Sun, S. H. Xie, B. Y. Bai, Y. X. Liu, K. M. Ji, J. H. Li, *J. Phys. Chem. C*, **2014**, 118, 14913.
- [20] H. Arandiyán, H. X. Dai, K. M. Ji, H. Y. Sun, J. H. Li, *ACS Catal.*, **2015**, 5, 1781.
- [21] B. Y. Bai, J. H. Li, J. M. Hao, *Appl. Catal. B*, **2015**, 164, 241.
- [22] Y. Le, D. P. Guo, B. Cheng, J. G. Yu, *Appl. Surf. Sci.*, **2013**, 274, 110.
- [23] Q. B. Wen, C. Q. Li, Z. H. Cai, W. Zhang, H. L. Gao, L. J. Chen, G. M. Zeng, X. Shu, Y. P. Zhao, *Bioresour. Technol.*, **2011**, 102, 942.
- [24] C. J. Ma, X. H. Li, T. L. Zhu, *Carbon*, **2011**, 49, 2873.
- [25] L. D. Zou, Y. G. Luo, M. Hooper, E. Hu, *Chem. Eng. Process*, **2006**, 45, 959.
- [26] J. Li, Z. Li, B. Liu, Q. B. Xia, H. X. Xi, *Chin. J. Chem. Eng.*, **2008**, 16, 871.
- [27] D. Chen, Z. P. Qu, Y. H. Sun, Y. Wang, *Colloid Surf. A*, **2014**, 441, 433.
- [28] A. Rezaee, H. Rangkooy, A. Jonidi-Jafari, A. Khavanin, *Appl. Surf. Sci.*, **2013**, 286, 235.
- [29] H. Q. Rong, Z. Y. Ryu, J. T. Zheng, Y. L. Zhang, *Carbon*, **2002**, 40, 2291.
- [30] K. J. Lee, N. Shiratori, G. H. Lee, J. Miyawaki, I. Mochida, S. H. Yoon, J. Jang, *Carbon*, **2010**, 48, 4248.
- [31] D. Chen, Z. P. Qu, W. W. Zhang, X. Y. Li, Q. D. Zhao, Y. Shi, *Colloid Surf. A*, **2011**, 379, 136.
- [32] K. Kosuge, S. Kubo, N. Kikukawa, M. Takemori, *Langmuir*, **2007**, 23, 3095.
- [33] Y. W. Lu, D. H. Wang, C. F. Ma, H. C. Yang, *Build. Environ.*, **2010**, 45, 615.
- [34] R. Akbarzadeh, S. B. Umbarkar, R. S. Sonawane, S. Takle, M. K. Dongare, *Appl. Catal. A*, **2010**, 374, 103.
- [35] P. A. Bourgeois, E. Puzenat, L. Peruchon, F. Simonet, D. Chevalier, E. Deflin, C. Brochier, C. Guillard, *Appl. Catal. B*, **2012**, 128, 171.
- [36] P. F. Fu, P. Y. Zhang, J. Li, *Appl. Catal. B*, **2011**, 105, 220.
- [37] G. K. Zhang, Q. Xiong, W. Xu, S. Guo, *Appl. Clay. Sci.*, **2014**, 102, 231.
- [38] Y. You, S. Y. Zhang, L. Wan, D. F. Xu, *Appl. Surf. Sci.*, **2012**, 258, 3469.
- [39] X. B. Zhu, D. L. Chang, X. S. Li, Z. G. Sun, X. Q. Deng, A. M. Zhu, *Chem. Eng. J.*, **2015**, 279, 897.
- [40] W. Low, V. Boonamnuayvitaya, *J. Environ. Manage.*, **2013**, 127, 142.
- [41] M. Khanmohammadi, A. B. Garmarudi, H. Elmizadeh, M. B. Roochi, *J. Ind. Eng. Chem.*, **2014**, 20, 1841.
- [42] B. Y. Bai, H. Arandiyán, J. H. Li, *Appl. Catal. B*, **2013**, 142–143, 677.
- [43] J. Quiroz Torres, S. Royer, J. P. Bellat, J. M. Giraudon, J. F. Lamoniér, *ChemSusChem*, **2013**, 6, 578.
- [44] C. B. Zhang, H. He, K. I. Tanaka, *Appl. Catal. B*, **2006**, 65, 37.
- [45] C. B. Zhang, H. He, *Catal. Today*, **2007**, 126, 345.
- [46] C. B. Zhang, F. D. Liu, Y. P. Zhai, H. Ariga, N. Yi, Y. C. Liu, K. Asakura, M. Flytzani-Stephanopoulos, H. He, *Angew. Chem. Int. Ed.*, **2012**, 51, 9628.
- [47] L. H. Nie, J. G. Yu, X. Y. Li, B. Cheng, G. Liu, M. Jaroniec, *Environ. Sci. Technol.*, **2013**, 47, 2777.
- [48] S. S. Kim, K. H. Park, S. C. Hong, *Appl. Catal. A*, **2011**, 398, 96.
- [49] N. H. An, W. L. Zhang, X. L. Yuan, B. Pan, G. Liu, M. J. Jia, W. F. Yan, W. X. Zhang, *Chem. Eng. J.*, **2013**, 215–216, 1.
- [50] J. X. Peng, S. D. Wang, *Appl. Catal. B*, **2007**, 73, 282.
- [51] K. T. Chuang, B. Zhou, S. M. Tong, *Ind. Eng. Chem. Res.*, **1994**, 33, 1680.
- [52] H. B. Huang, D. Y. C. Leung, *J. Catal.*, **2011**, 280, 60.
- [53] H. B. Huang, D. Y. C. Leung, *ACS Catal.*, **2011**, 1, 348.
- [54] S. J. Park, I. Bae, I. S. Nam, B. K. Cho, S. M. Jung, J. H. Lee, *Chem. Eng. J.*, **2012**, 195–196, 392.
- [55] V. A. dela O'Shea, M. Cálvarez-Galván, J. L. G. Fierro, P. L. Arias, *Appl. Catal. B*, **2005**, 57, 191.
- [56] Z. P. Qu, S. J. Shen, D. Chen, Y. Wang, *J. Mol. Catal. A*, **2012**, 356, 171.
- [57] C. F. Mao, M. A. Vannice, *J. Catal.*, **1995**, 154, 230.
- [58] S. Imamura, D. Uchihori, K. Utani, T. Ito, *Catal. Lett.*, **1994**, 24, 377.
- [59] K. Sekizawa, H. Widjaja, S. Maeda, Y. Ozawa, K. Eguchi, *Appl. Catal. A*, **2000**, 200, 211.
- [60] S. Minicò, S. Scirè, C. Crisafulli, R. Maggiore, S. Galvagno, *Appl. Catal. B*, **2000**, 28, 245.
- [61] S. Imamura, Y. Uematsu, K. Utani, T. Ito, *Ind. Eng. Chem. Res.*, **1991**, 30, 18.
- [62] X. F. Tang, J. L. Chen, X. M. Huang, Y. D. Xu, W. J. Shen, *Appl. Catal. B*, **2008**, 81, 115.
- [63] X. F. Tang, J. L. Chen, Y. G. Li, Y. Li, Y. D. Xu, W. J. Shen, *Chem. Eng. J.*, **2006**, 118, 119.
- [64] Y. N. Shen, X. Z. Yang, Y. Z. Wang, Y. B. Zhang, H. Y. Zhu, L. Gao, M. L. Jia, *Appl. Catal. B*, **2008**, 79, 142.
- [65] H. F. Li, N. Zhang, P. Chen, M. F. Luo, J. Q. Lu, *Appl. Catal. B*, **2011**, 110, 279.
- [66] C. Y. Li, Y. N. Shen, M. L. Jia, S. S. Sheng, M. O. Adebajo, H. Y. Zhu, *Catal. Commun.*, **2008**, 9, 355.
- [67] N. H. An, Q. S. Yu, G. Liu, S. P. Li, M. J. Jia, W. X. Zhang, *J. Hazard. Mater.*, **2011**, 186, 1392.
- [68] H. Tian, J. H. He, L. L. Liu, D. H. Wang, *Ceram. Int.*, **2013**, 39, 315.
- [69] X. H. Yu, J. H. He, D. H. Wang, Y. C. Hu, H. Tian, Z. C. He, *J. Phys. Chem. C*, **2011**, 116, 851.
- [70] Z. W. Huang, G. Xu, Q. Q. Cao, P. P. Hu, J. M. Hao, J. H. Li, X. F. Tang, *Angew. Chem. Int. Ed.*, **2012**, 51, 4198.
- [71] P. P. Hu, Z. Amghouz, Z. W. Huang, F. Xu, Y. X. Chen, X. F. Tang,

- Environ. Sci. Technol.*, **2015**, 49, 2384.
- [72] J. Zhang, Y. Jin, C. Y. Li, Y. N. Shen, L. Han, Z. X. Hu, X. W. Di, Z. L. Liu, *Appl. Catal. B*, **2009**, 91, 11.
- [73] B. C. Liu, C. Y. Li, Y. F. Zhang, Y. Liu, W. T. Hu, Q. Wang, L. Han, J. Zhang, *Appl. Catal. B*, **2012**, 111, 467.
- [74] B. C. Liu, Y. Liu, C. Y. Li, W. T. Hu, P. Jing, Q. Wang, J. Zhang, *Appl. Catal. B*, **2012**, 127, 47.
- [75] C. Y. Ma, D. H. Wang, W. J. Xue, B. J. Dou, H. L. Wang, Z. P. Hao, *Environ. Sci. Technol.*, **2011**, 45, 3628.
- [76] C. Y. Ma, Z. Mu, J. J. Li, Y. G. Jin, J. Cheng, G. Q. Lu, Z. P. Hao, S. Z. Qiao, *J. Am. Chem. Soc.*, **2010**, 132, 2608.
- [77] Y. B. Zhang, Y. N. Shen, X. G. Yang, S. S. Sheng, T. Wang, M. F. Adebajo, H. Y. Zhu, *J. Mol. Catal. A*, **2010**, 316, 100.
- [78] B. Y. Bai, J. H. Li, *ACS Catal.*, **2014**, 4, 2753.
- [79] L. Ma, D. S. Wang, J. H. Li, B. Y. Bai, L. X. Fu, Y. D. Li, *Appl. Catal. B*, **2014**, 148–149, 36.
- [80] R. H. Wang, J. H. Li, *Catal. Lett.*, **2009**, 131, 500.
- [81] Y. Sekine, A. Nishimura, *Atmos. Environ.*, **2001**, 35, 2001.
- [82] Y. Sekine, *Atmos. Environ.*, **2002**, 36, 5543.
- [83] L. Zhou, J. Zhang, J. H. He, Y. C. Hu, H. Tian, *Mater. Res. Bull.*, **2011**, 46, 1714.
- [84] T. Chen, H. Y. Dou, X. L. Li, X. F. Tang, J. H. Li, J. M. Hao, *Microporous Mesoporous Mater.*, **2009**, 122, 270.
- [85] Y. Xu, J. Greeley, M. Mavrikakis, *J. Am. Chem. Soc.*, **2005**, 127, 12823.
- [86] X. W. Xie, Y. Li, Z. Q. Liu, M. Haruta, W. J. Shen, *Nature*, **2009**, 458, 746.
- [87] D. Widmann, R. J. Behm, *Angew. Chem. Int. Ed.*, **2011**, 50, 10241.
- [88] H. M. Chen, J. H. He, C. B. Zhang, H. He, *J. Phys. Chem. C*, **2007**, 111, 18033.
- [89] X. F. Tang, X. M. Huang, J. J. Shao, J. L. Liu, Y. G. Li, Y. D. Xu, W. J. Shen, *Chin. J. Catal.*, **2006**, 27, 97.
- [90] H. Tian, J. H. He, X. D. Zhang, L. Zhou, D. H. Wang, *Microporous Mesoporous Mater.*, **2011**, 138, 118.
- [91] H. Tian, J. H. He, L. L. Liu, D. H. Wang, Z. P. Hao, C. Y. Ma, *Microporous Mesoporous Mater.*, **2012**, 151, 397.
- [92] Y. S. Xia, H. X. Dai, L. Zhang, J. G. Deng, H. He, C. T. Au, *Appl. Catal. B*, **2010**, 100, 229.
- [93] B. Y. Bai, J. H. Li, J. M. Hao, *Appl. Catal. B*, **2015**, 164, 241.
- [94] B. Y. Bai, Q. Qiao, J. H. Li, J. M. Hao, *Chin. J. Catal.*, **2015**, 36, 27.
- [95] X. F. Tang, Y. G. Li, X. M. Huang, Y. D. Xu, H. Q. Zhu, J. G. Wang, W. J. Shen, *Appl. Catal. B*, **2006**, 62, 265.
- [96] X. S. Liu, J. Q. Lu, K. Qian, W. X. Huang, M. F. Luo, *J. Rare. Earth*, **2009**, 27, 418.
- [97] Y. R. Wen, X. Tang, J. H. Li, J. M. Hao, L. S. Wei, X. F. Tang, *Catal. Commun.*, **2009**, 10, 1157.
- [98] J. J. Pei, X. Han, Y. Lu, *Build. Environ.*, **2015**, 84, 134.
- [99] L. Bai, F. Wyrwalski, J. F. Lamonier, A. Y. Khodakov, E. Monflier, A. Ponchel, *Appl. Catal. B*, **2013**, 138–139, 381.
- [100] Y. Wang, A. M. Zhu, B. B. Chen, M. Crocker, C. Shi, *Catal. Commun.*, **2013**, 36, 52.
- [101] H. Arandiyani, H. X. Dai, J. G. Deng, Y. Wang, H. Y. Sun, S. H. Xie, B. Y. Bai, Y. X. Liu, K. M. Ji, J. H. Li, *J. Phys. Chem. C*, **2014**, 118, 14913.
- [102] H. Arandiyani, H. X. Dai, K. M. Ji, H. Y. Sun, J. H. Li, *ACS Catal.*, **2015**, 5, 1781.
- [103] H. Over, A. P. Seitsonen, *Science*, **2002**, 297, 2003.
- [104] K. An, S. Alayoglu, N. Musselwhite, S. Plamthottam, G. Melaet, A. E. Lindeman, G. A. Somorjai, *J. Am. Chem. Soc.*, **2013**, 135, 16689.
- [105] J. H. Li, R. H. Wang, J. M. Hao, *J. Phys. Chem. C*, **2010**, 114, 10544.
- [106] Y. X. Liu, H. X. Dai, J. G. Deng, S. H. Xie, H. G. Yang, W. Tan, W. Han, Y. Jiang, G. S. Guo, *J. Catal.*, **2014**, 309, 408.

甲醛催化氧化催化剂的研究进展

拜冰阳^{a,b,#}, 乔琦^{a,b}, 李俊华^{c,*}, 郝吉明^c

^a中国环境科学研究院环境基准与风险评估国家重点实验室, 北京100012

^b中国环境科学研究院国家环境保护生态工业重点实验室, 北京100012

^c清华大学环境学院环境模拟与污染控制国家重点联合实验室, 北京100084

摘要: 甲醛是致癌致畸物并具有较强的光化学活性。它既来源于纺织、农药、板材或其他精细化学品的生产过程, 又来源于机动车尾气和室内各种装潢材料。为了人体健康和大气环境去除甲醛非常必要。用催化氧化法去除甲醛是一种很有前景的技术, 但是该技术的关键是研究和开发催化剂。近年来, 用于甲醛氧化的催化剂主要分为贵金属催化剂和过渡金属氧化物催化剂。

贵金属催化剂是将Pt, Pd, Au, Ag等贵金属负载在不同类型的载体上而制得。载体可分为常见载体、传统金属氧化物载体和特殊形貌金属氧化物载体。常见载体是具有较大比表面积的SiO₂, Al₂O₃, TiO₂和分子筛等。这类载体有利于活性位的暴露以及反应物和产物的吸附和扩散, 而且还能增强载体和活性组分的协同作用。负载在常见载体上的不同贵金属催化剂, 其甲醛氧化活性从强到弱排列是: Pt > Pd > Rh > Au > Ag。用这种载体制备的催化剂具有很出色的应用前景。比如Na-Pt/TiO₂是甲醛氧化活性最好的催化剂, 目前已被应用在空气净化器中, 其次是Pt/TiO₂和Pd/TiO₂。传统金属氧化物载体主要是采用沉淀法、共沉淀法制备的CeO₂, Fe₂O₃, Co₃O₄, MnO₂及其复合氧化物, 这类载体负载Pt的催化剂仍然具有出色的室温催化性能, 如Pt/MnO_x-CeO₂和Pt/Fe₂O₃等。虽然Pt负载型催化剂应用前景很好, 但是其成本较高, 工业生产和普及受到限制。用传统金属氧化物载体制备的催化剂如Au/CeO₂, Ag/MnO_x-CeO₂和Ag/CeO₂等同样具有良好的发展前景。对于提高甲醛氧化活性来说, 载体的选择至关重要。未来研究趋势可能是甲醛氧化负载型催化剂更多的会选择Ag或Au作为活性组分, 而一些有潜力的传统金属氧化物载体将被使用不同的制备方法进一步改良。目前, 拥有棒状、球状、孔状等特殊形貌的金属氧化物载体因为它们本身的催化活性要优于用沉淀法制备的传统金属氧化物催化剂, 因此, 将Ag或Au负载在这类载体上制备的催化剂具有更好的应用前景, 如三维(3D)有序大孔Au/CeO₂-Co₃O₄, 二维有序介孔Au/Co₃O₄-CeO₂和Au/Co₃O₄

以及三维有序介孔K-Ag/Co₃O₄等。

过渡金属氧化物催化剂,因成本低,资源丰富而受到关注.单一过渡金属氧化物催化剂如锰钾矿型的MnO₂纳米棒或纳米球,介孔MnO₂,Co₃O₄和Cr₂O₃等,具有较好的甲醛氧化催化活性(T_{50} 和 T_{100} 分别小于等于110和140 °C).另外,Ce,Sn,Cu和Zr等元素常常被掺杂到MnO_x和Co₃O₄中,制备成复合金属氧化物催化剂,MnO_x-CeO₂具有较好的甲醛催化活性($T_{50} < 100$ °C),因为MnO_x和CeO₂较强的相互作用改变了表面活性氧和活性相的数量.目前,复合金属氧化物催化剂氧化甲醛的报道很少.随着制备方法的改变,单一过渡金属氧化物或他们的复合氧化物催化剂可能会成为贵金属催化剂的替代品.

目前,如何获得高效、低成本、低温甚至常温去除甲醛的催化剂仍然是一项重要的挑战.特殊形貌的金属氧化物催化剂如3D-Cr₂O₃,3D-Co₃O₄,MnO₂纳米球和纳米棒,在常温下完全转化甲醛仍然是个难以越过的鸿沟.

将来,多种形貌的新型纳米金属氧化物及其Au或Ag负载型催化剂的制备和发展会成为一个研究趋势.这种催化剂既能被用于甲醛的催化氧化,也能被用于苯系物或其他VOCs的催化氧化.它能为机动车尾气和工业生产中VOCs产生量的削减提供技术支撑,而VOCs的去除有益于PM_{2.5}浓度的降低和空气质量的恢复.

关键词: 甲醛; 催化氧化; 金属氧化物催化剂; 贵金属催化剂; 低温催化活性

收稿日期: 2015-08-27. 接受日期: 2015-10-20. 出版日期: 2016-01-05.

*通讯联系人. 电话/传真: (010)62771093; 电子信箱: lijunhua@tsinghua.edu.cn

#通讯联系人. 电话: (010)84914902; 传真: (010)84914626; 电子信箱: baibingyang@tsinghua.org.cn

基金来源: 国家自然科学基金(21325731, 51478241, 21221004).

本文的英文电子版由Elsevier出版社在ScienceDirect上出版(<http://www.sciencedirect.com/science/journal/18722067>).